

**The special role of the first Matsubara frequency for
superconductivity near a quantum-critical point – the non-linear
gap equation below T_c and spectral properties in real frequencies**

Yi-Ming Wu,¹ Artem Abanov,² Yuxuan Wang,³ and Andrey V. Chubukov¹

¹*School of Physics and Astronomy and William I. Fine Theoretical Physics Institute,
University of Minnesota, Minneapolis, MN 55455, USA*

²*Department of Physics, Texas A&M University, College Station, USA*

³*Department of Physics, University of Florida, Gainesville, FL 32611, USA*

(Dated: December 20, 2018)

Abstract

Near a quantum-critical point in a metal a strong fermion-fermion interaction, mediated by a soft boson, destroys fermionic coherence and also gives rise to an attraction in one or more pairing channels. The two tendencies compete with each other, and in a class of large N models, where the tendency to incoherence is parametrically stronger, one would naively expect an incoherent (non-Fermi liquid) normal state behavior to persist down to $T = 0$. However, this is not the case for quantum-critical systems described by Eliashberg theory. In such systems, non-Fermi liquid part of the self-energy $\Sigma(\omega_m)$ is large for a generic Matsubara frequency $\omega_m = \pi T(2m + 1)$, but vanishes for fermions with $\omega_m = \pm\pi T$, while the pairing interaction between fermions with these two frequencies remains strong. It has been shown [Y. Wang *et al* PRL 117, 157001 (2016)] that this peculiarity gives rise to a non-zero T_c , even at large N , when superconductivity is not expected from scaling analysis. We consider the system behavior below T_c and contrast the conventional case, when $\omega_m = \pm\pi T$ are not special, and the case when the pairing is induced by fermions with $\omega_m = \pm\pi T$. We obtain the solution of the non-linear gap equations in Matsubara frequencies and then convert to real frequency axis and obtain the spectral function $A(\omega)$ and the density of states $N(\omega)$. In a conventional BCS-type superconductor $A(\omega)$ and $N(\omega)$ are peaked at the gap value $\Delta(T)$, and the peak position shifts to a smaller ω as temperature increases towards T_c , i.e. the gap “closes in”. We show that in a situation when superconductivity is induced by fermions with $\omega_m = \pm\pi T$, the peak $N(\omega)$ remains at a finite frequency even at $T = T_c - 0$, the gap just “fills in”. The spectral function $A(\omega)$ either shows almost the same “gap filling” behavior as the density of states, or its peak position shifts to zero frequency already at a finite Δ (“emergent Fermi arc” behavior), depending on the strength of the thermal contribution. We compare our results with the data for the cuprates and argue that “gap filling” behavior holds in the antinodal region, while the “emergent Fermi arc” behavior holds in the nodal region.

I. INTRODUCTION.

The pairing near a quantum-critical point (QCP) in a metal is a fascinating subject due to highly non-trivial interplay between superconductivity and non-Fermi liquid (NFL) behavior^{1? -33}. In most cases, the dominant interaction between low-energy fermions near a QCP is mediated by critical fluctuations of the order parameter. In dimensions $D \leq 3$, this

interaction gives rise to a singular fermionic self-energy, and a coherent Fermi-liquid behavior get destroyed below a certain temperature T_{coh} , either on the full Fermi surface^{13,15,34,35} or in the hot regions^{6-8,13,19,36,37}. The same interaction, however, also mediates fermion-fermion interaction in the particle-particle channel. The electron-mediated interaction is positive (repulsive), but it depends on both momentum and frequency and generally has at least one attractive component (d -wave for antiferromagnetic QCP, p -wave for a ferromagnetic QCP, s, p, d -wave for a nematic QCP, Ref.^{17,38}) If this system becomes superconducting below some finite T_c , the range of NFL behavior shrinks to $T_{coh} > T > T_c$, and even vanishes when $T_c > T_{coh}$ ¹⁸. A naked quantum-critical $T = 0$ behavior can only be observed either if the pairing interaction is repulsive, or if fermionic incoherence prevents superconductivity to develop down to $T = 0$.

In all known physical quantum-critical (QC) models of fermions, superconducting T_c is finite^{5,6,18,20,21,32,33}. This can be interpreted as an evidence that the tendency to pairing is stronger than towards incoherent, NFL behavior. The situation can potentially be reversed if the interaction in the pairing channel is somehow reduced compared to that in the particle-hole channel. This can be achieved by either modifying the momentum dependence of the interaction mediated by critical fluctuations to reduce the partial pairing component in the channel, where it is attractive, or by keeping the interaction intact but extending the model to an $SU(N)$ global symmetry²⁰ (the original model corresponds to $N = 1$). Under this extension, the pairing interaction get reduced by $1/N$, but the self-energy stays intact²⁰. In both cases, the functional form of equation for the (frequency dependent) pairing vertex in the attractive channel does not change, but the magnitude of the eigenvalue needed for superconductivity gets larger. The analysis of a large- N QC model at $T = 0$ shows^{20,21} that there exists a critical N_{cr} , separating a superconducting region at $N < N_{cr}$ and a region of a $T = 0$ NFL normal state behavior at $N > N_{cr}$ (see Fig. 1). A conventional reasoning in this situation would be that the superconducting $T_c(N)$ terminates at $T = 0$, $N = N_{cr}$, and vanishes for $N > N_{cr}$. However, numerical studies of large- N QC models yield a different result²¹ - T_c remains finite at any N , and the critical line $T_c(N)$ by-passes $N = N_{cr}$, and $T_c(N)$ remains finite at all N (see Fig. 2).

This unusual behavior was argued in Ref. 21 to be the consequence of the special form of Matsubara fermionic self-energy $\Sigma(\omega_m)$ at the two lowest Matsubara frequencies: $\omega_m = \pi T$ and $\omega_m = -\pi T$. Namely, in Eliashberg theory $\Sigma(\pm\pi T)$ only contains the self-action

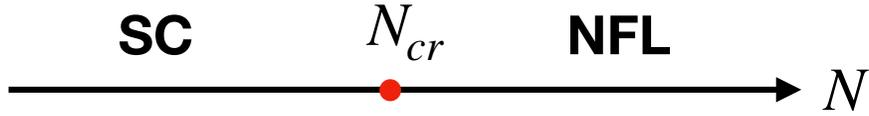


FIG. 1. The $T = 0$ phase diagram of an itinerant QC model with fermion-fermion interaction mediated by a critical boson with dynamical propagator $\chi(\Omega_m) = (g/|\Omega_m|)^\gamma$, where $0 < \gamma < 1$. The original model with $N = 1$ has been extended to $N > 1$ in such a way that the pairing interaction is reduced by $1/N$, while the interaction in the particle-hole channel (the one which gives rise to NFL behavior in the normal state) remains intact. The critical $N_{cr} = N_{cr}(\gamma) > 1$ separates the regions of superconductivity at $N < N_{cr}$ and NFL normal state behavior at $N > N_{cr}$.

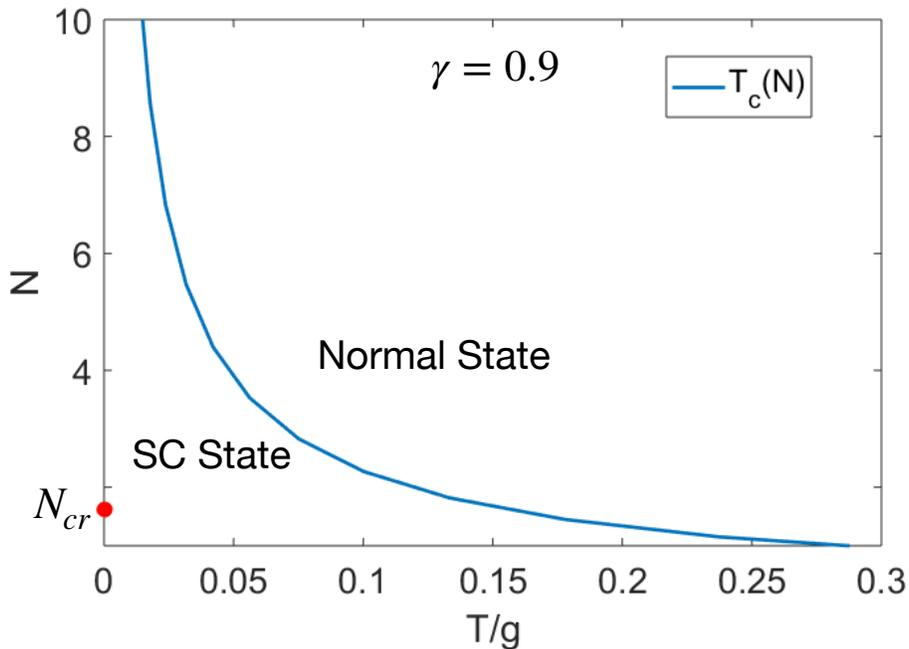


FIG. 2. The onset temperature of superconductivity, $T_c(N)$, in the QC model, extended to $N > 1$. We set $\gamma = 0.9$. The line $T_c(N)$ by-passes N_{cr} (the red dot). At large N , $T_c(N) \propto 1/N^{1/\gamma}$.

term (thermal contribution to $\Sigma(\omega_m)$ from zero bosonic Matsubara frequency), all other contributions cancel out. The thermal piece in $\Sigma(\omega_m)$ comes from scattering with zero frequency and finite momentum transfer and mimics the scattering by impurities. The same thermal scattering also contributes to the pairing vertex $\Phi(\omega_m)$. For spin-singlet pairing, the two contributions cancel out in equation for the gap function $\Delta(\omega_m) = \Phi(\omega_m)/(1 + \Sigma(\omega_m)/\omega_m)$ by Anderson's theorem^{39,40}. As a consequence, fermions with $\omega_m = \pm\pi T$ can be treated for the pairing as free quasiparticles. Meanwhile the pairing interaction between fermions with $\omega_m = \pi T$ and $\omega_m = -\pi T$ remains strong. This strong interaction, not countered by the self-energy, gives rise to the emergence of $\Delta(\pm\pi T)$ below a certain $T_c(N)$, which remains finite for all values of N . A finite $\Delta(\pm\pi T)$ then induces non-zero $\Delta(\omega_m)$ at other Matsubara frequencies, for which the self-energy without self-action is strong.

In this communication we extend the analysis of superconductivity induced by first fermionic Matsubara frequencies to $T < T_c(N)$. We argue that, although $T_c(N)$ by-passes $N = N_{cr}$, there is a crossover in the system behavior at $T_{cross}(N) < T_c(N)$. The crossover line $T_{cross}(N)$ originates at $T = 0$ for $N = N_{cr}$ and ends at $T_{cross} \leq T_c$ for the physical case $N = 1$. At $T_{cross}(N) < T < T_c(N)$, superconductivity can be viewed as induced by fermions with $\omega_m = \pm\pi T$, at smaller $T < T_{cross}(N)$ fermions with all ω_m contribute to superconductivity, and the ones with $\omega_m = \pm\pi T$ are no longer special. We show the schematic phase diagram in Fig. 3.

We analyze the evolution of the gap $\Delta(\omega_m)$ below $T_c(N)$ at $N > N_{cr}$ and $N < N_{cr}$ and then convert from Matsubara to real frequencies and analyze the behavior of $\Delta(\omega)$, the spectral function at the Fermi surface $A(\omega)$, and the density of states (DOS) $N(\omega)$. We argue that the system behavior below $T_c(N)$ is different for $N > N_{cr}$ and $N < N_{cr}$ (see the paths (a) and (b) in Fig.3). At $N > N_{cr}$ it is qualitatively different from BCS. At $N < N_{cr}$, the system behavior is similar to a BCS superconductor for $T < T_{cross}(N)$ and to that at $N > N_{cr}$ for $T > T_{cross}(N)$.

Along the Matsubara axis, we find that at large $N > N_{cr}$, the pairing vertex $\Phi(\omega_m)$ is smaller than $\Sigma(\omega_m)$ for all temperatures and all Matsubara frequencies, including $\pm\pi T$. In fact, $\Sigma(\omega_m)$ with $m \neq 0, -1$ remains essentially the same as in the normal state, i.e., the feedback effect from superconductivity on this self-energy is weak. The self-energy $\Sigma(\pm\pi T)$ becomes finite below $T_c(N)$, but remains smaller by $1/N$ than $\Sigma(\omega_m)$ at other Matsubara frequencies. Still, it is larger by \sqrt{N} than $\Phi(\pm\pi T)$. We show that in this situation, $\Delta(\omega_m, T)$

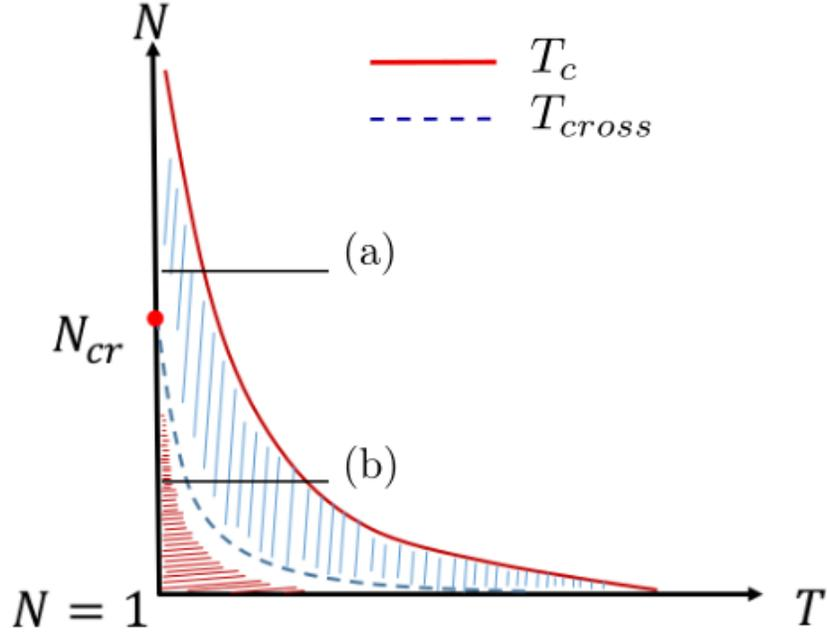


FIG. 3. A schematic phase diagram of our QC model, extended to $N > 1$, for some $\gamma < 1$. The solid line is the onset temperature for superconductivity, $T_c(N)$. The dashed line marks the crossover from the behavior similar to a BCS superconductor at a lower T to the novel behavior at a higher T , in which superconducting order does not provide a substantial feedback effect on the fermionic self-energy, and it largely remains the same as in the normal state. In this region, the spectral function $A(\omega)$ and the DOS $N(\omega)$ are functions of ω/T rather than of $\omega/\Delta(T)$. The critical N_{cr} separates superconducting and normal states at $T = 0$. This phase diagram has been obtained within the Eliashberg theory and does not include phase fluctuations. The latter likely destroy long-range superconducting order in some T range below $T_c(N)$. Our results for $N(\omega)$ and $A(\omega)$ above the crossover line should survive in this range as they do not rely on the existence of a long-range superconducting order.

is monotonic as a function of ω_m , with the largest value at $\pm\pi T$, but non-monotonic as a function of temperature, i.e., $\Delta(\pi T)$ first increases when T decreases below $T_c(N)$, then passes through a maximum and eventually vanishes at $T = 0$. At $N < N_{cr}$, $\Delta(\pi T)$ becomes non-zero at $T = 0$, and its magnitude increases as N gets progressively smaller than N_{cr} . At $N \leq N_{cr}$, the temperature dependence of $\Delta(\pi T)$ is still non-monotonic, with the maximum

at a finite T . At smaller N , the maximum becomes more shallow, and at $N \gtrsim 1$, $\Delta(\pi T)$ monotonically increases with decreasing T .

We use the results along the Matsubara axis as an input and obtain the behavior of $\Phi(\omega)$ and $\Sigma(\omega)$ along real frequency axis. Using these $\Phi(\omega)$ and $\Sigma(\omega)$, we obtain the DOS

$$N(\omega) = N_0 \operatorname{Re} \left[\frac{1}{\sqrt{1 - (\Phi(\omega)/(\omega + \Sigma(\omega)))^2}} \right] \quad (1)$$

The thermal contributions to $\Phi(\omega)$ and to $\omega + \Sigma(\omega)$ are the same and they cancel out in the DOS, i.e., in the calculations one can replace $\Phi(\omega)$ and $\Sigma(\omega)$ by $\Phi^*(\omega)$ and $\Sigma^*(\omega)$, which are the solutions of the Eliashberg equations with thermal contributions explicitly taken out. We show that, for $N > N_{cr}$, $N(\omega)$ is finite for all frequencies, including $\omega = 0$, and its dependence on ω is determined by a universal scaling function of ω/T . As the consequence, the frequency at which $N(\omega)$ has a maximum, linearly increases with increasing T . As T approaches T_c from below, DOS “fills in”, i.e., the $N(\omega)$ approaches N_0 , but the position of the maximum in $N(\omega)$ remains at a finite frequency.

At $N < N_{cr}$, the DOS $N(\omega)$ at the lowest $T < T_{cross}(N)$ displays a sharp gap, , i.e., it nearly vanishes at $\omega < \omega_0$, where ω_0 is roughly equal to $\Delta(0)$ (more exactly, ω_0 is the solution of $\Delta(\omega_0) = \omega_0$). As T increases, the position of the maximum in the DOS initially shifts to a lower frequency, as in a BCS superconductor, because $\Delta(0)$ gets smaller with increasing T , i.e., the gap in the DOS “closes in” with increasing temperature. However, once temperature exceeds $T_{cross}(N)$, this behavior changes and becomes the same as for larger N , i.e., at these T the the position of the maximum in DOS shifts to a higher frequency with increasing T and remains finite at $T = T_c(N) - 0$, i.e., the DOS “fills in” with increasing T . We emphasize that these two distinct regimes of system behavior are present also in the original physical model with $N = 1$. In this respect, the extension to $N > 1$ is just a convenient way to understand the origin of such behavior by extending the regime in which superconductivity is generated by fermions with $\omega = \pm\pi T$. A representative of our results for the DOS is shown in Fig.4 The behavior of the spectral function is more involved because in $A(\omega)$ the thermal contribution does not cancel out. The expression for $A(\omega) = -(1/\pi) \operatorname{Im}[G(k_F, \omega)]$

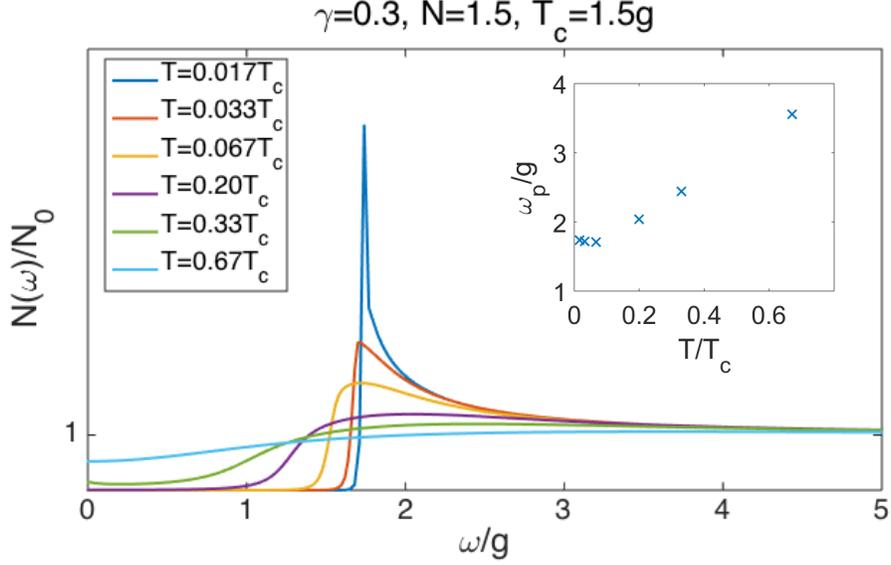


FIG. 4. A representative of our results for the DOS. We set $\gamma = 0.3$ and $N = 1.5$, which is smaller than N_{cr} for this γ . At low $T < T_{cross} \sim 0.1T_c$, the DOS has a peak at $\omega \approx \Delta(T)$, and the peak frequency decreases as temperature increases, i.e. the gap in the DOS closes. At $T > T_{cross}$ the DOS flattens up with increasing T (the gap fills in). In this T range the maximum in the DOS is located at $\omega_p \sim T$, which increases with increasing T .

at $\omega > 0$ is (see Eq.(68) below)

$$A(\omega) = \frac{1}{\pi} \text{Im} \left[\frac{\omega + \Sigma^*(\omega)}{(\omega + \Sigma^*(\omega))^2 - \Phi^*(\omega)^2} L(\omega) \right] \quad (2)$$

$$L(\omega) = \frac{\sqrt{(\omega + \Sigma^*(\omega))^2 - \Phi^*(\omega)^2}}{iP + \sqrt{(\omega + \Sigma^*(\omega))^2 - \Phi^*(\omega)^2}}$$

where frequency-independent $P = P(T)$ describes the thermal contribution to self-energy, and $\Sigma^*(\omega)$, $\Phi^*(\omega)$ are obtained from $\Sigma(\omega)$, $\Phi(\omega)$ by excluding thermal contributions (see (44) and the Appendix for more details). For large P , $A(\omega) \propto N(\omega)$, i.e., the spectral function displays the same crossover from “gap closing” to “gap filling” as the DOS. For smaller P , when the term next to P in (2) is larger than P , $A(\omega)$ at $T < T_{cross}$ shows two sharp peaks at $\omega = \pm\omega_0$. At temperatures above T_{cross} , the two peaks merge, and $A(\omega)$ develops a maximum at $\omega = 0$, like in the normal state. A representative of our results for $A(\omega)$ is shown in Fig.5.

The transformation from “gap closing” to “gap filling” behavior in the DOS has been

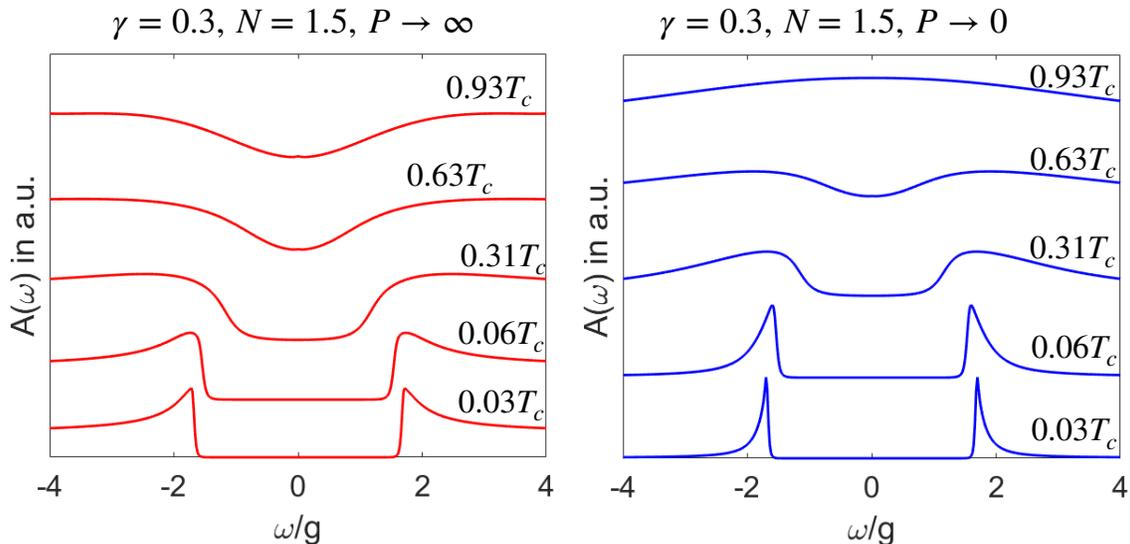


FIG. 5. A representative of our results for the spectral function $A(\omega)$ for $\gamma = 0.3$ and $N = 1.5$ ($N < N_{cr}$). Left panel is for the case when thermal contribution to $A(\omega)$ is strong, right panel is for the case when it is weak (in our notations, the cases $P \rightarrow \infty$ and $P \approx 0$, respectively). In both panels, $A(\omega)$ at low $T < T_{cross}$ has well pronounced peaks at $\omega = \pm\Delta(T)$. The peak frequency decreases with increasing T . At $T > T_{cross}$, the peaks disappear, and the spectral function shows a dip, when P is large, and a single peak at $\omega = 0$, when P is small. For cuprate superconductors, we associate the spectral function in the right panel with that of antinodal fermions, and the one in the left panel with the spectral function of fermions in near-nodal, Fermi arc region.

observed in several superconducting materials, most notably the cuprates^{41–50} The spectral function in the cuprates shows the same behavior as the DOS in the antinodal regions, where the fermionic incoherence is the strongest, and the d -wave gap is the largest. In the regions near the Brillouin zone diagonals, the symmetrized spectral function has peaks at a finite frequency $\pm\omega_0$ at low temperatures, and a single maximum at $\omega = 0$ at higher temperatures. The angular range in which the system displays a single peak above a certain T is termed as a Fermi arc⁴⁵.

The crossover from “gap closing” to “gap filling” in the DOS and in $A(\omega)$ in the antinodal regions, and the crossover from two peaks to a single peak in $A(\omega)$ in the nodal regions, have been phenomenologically described by assuming that the pairing vertex $\Phi^*(\omega) = \Delta(T)$, as in a BCS superconductor, and $\Sigma^*(\omega) = i\Gamma(T)$ (Refs.^{51–53}) Under these approximation, the

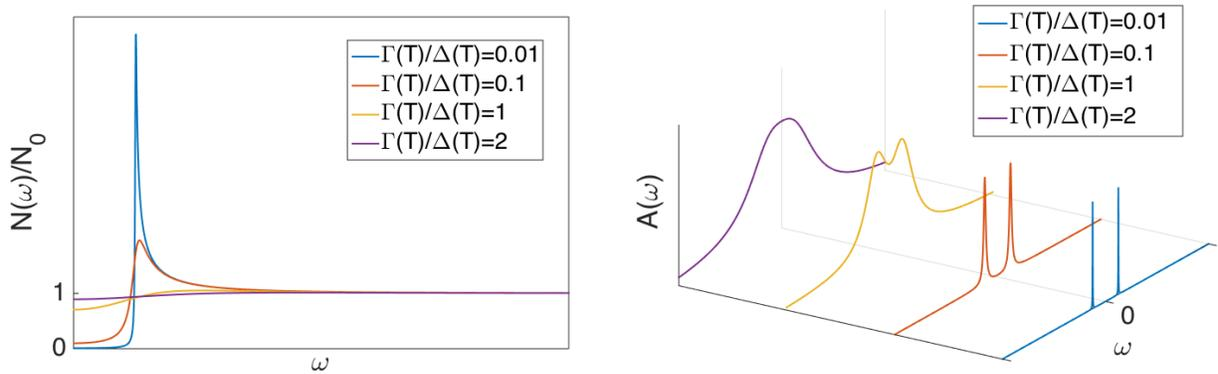


FIG. 6. The DOS $N(\omega)$ and the spectral function $A(\omega)$ in a dirty BCS superconductor, from Eq. (3) and Eq. (4).

DOS becomes

$$N(\omega) = N_0 \operatorname{Re} \left[\frac{1}{\sqrt{1 - \left(\frac{\Delta(T)}{\omega + i\Gamma(T)} \right)^2}} \right] \quad (3)$$

Without $\Gamma(T)$, the DOS vanishes at $\omega < \Delta$ and is singular at $\omega = \Delta + 0$. A non-zero $\Gamma(T)$ makes $N(\omega)$ continuous and non-zero down to $\omega = 0$. Furthermore, the position of the peak in $N(\omega)$ shifts to a higher frequency from $\omega = \Delta(T)$ (see Fig.6) At vanishing $\Delta(T)$ the peak in $N(\omega) \approx N_0 \left(1 + \frac{1}{2} \Delta^2 \operatorname{Re} \left[\frac{1}{(\omega + i\Gamma)^2} \right] \right)$ remains at a finite $\omega = \sqrt{3}\Gamma$. In other words, the magnitude of the deviation of $N(\omega)$ from N_0 is set by Δ^2 , while its frequency dependence is set by $\operatorname{Re} \frac{1}{(\omega + i\Gamma)^2}$ and does not depend on Δ . If one additionally sets $\Gamma = O(T)$, as in marginal FL theory, one obtains that the position of the maximum in the DOS increases linearly with T near $T = T_c$, when $\Gamma > \Delta(T)$. The same phenomenological model with $\Gamma(T) \propto T$ was used⁵³ to explain Fermi arcs (assuming that the thermal contribution can be neglected). Indeed, at $P = 0$, we have from (2)

$$\begin{aligned} A(\omega) &= -\frac{1}{\pi} \operatorname{Im} \left[\frac{\omega + i\Gamma(T)}{(\omega + i\Gamma(T))^2 - \Delta^2(T)} \right] \\ &= \frac{1}{\pi} \frac{\omega^2 + \Delta^2(T) + \Gamma^2(T)}{(\omega^2 - \Delta^2(T) - \Gamma^2(T))^2 + 4\omega^2\Gamma^2(T)} \end{aligned} \quad (4)$$

This spectral function has two separate peaks at positive and negative ω at $\Gamma(T) < \sqrt{3}\Delta(T)$, and a single maximum at $\omega = 0$ at $\Gamma(T) > \sqrt{3}\Delta(T)$ (Fig.6)

This phenomenon when $N(0)$ becomes finite is known as “gapless superconductivity”. It

was originally found by Abrikosov and Gorkov in their analysis of an s -wave BCS superconductor with magnetic impurities⁵⁴. At $T = 0$, gapless superconductivity exists in a finite parameter range before magnetic impurities destroy superconductivity. Several researchers later argued⁵⁵ that any phonon-mediated s -wave superconductor at a finite T is a gapless superconductor due to scattering on thermally excited phonons, although in practice Γ due to such scattering is extremely small at small coupling. For electronically-mediated superconductivity in a clean metal, self-energy $\Sigma(\omega)$ in the normal state contains the imaginary part. In a superconducting state, the imaginary part of $\Sigma(\omega)$ is reduced at $\omega < \Delta$ due to the reduction of the phase space for low-energy scattering. This holds for any symmetry of the gap function and gives rise to peak-dip-hump feature of the spectral functions, studied extensively in the cuprates^{45,56-58}. As long as T is finite, $\Sigma''(\omega = 0)$ remains non-zero, but at low T it gets substantially reduced compared to its value at $T = T_c$. Numerical analysis of Eliashberg equations for several models of magnetically-induced d -wave superconductivity^{7,16,36} and for strong coupling (small Debye frequency) limit of electron-phonon superconductivity¹⁻⁴ did find that $\Sigma''(0)$ rapidly increases at T near T_c , and the maximum in the theoretical DOS shifts up from $\Delta(T)$ and remains at a finite frequency at $\sim T_c$, where $\Delta(T)$ vanishes in the Eliashberg theory. This is roughly consistent with the phenomenology of Eq. (3), although temperature variation of the peak position in the DOS has not been explicitly verified.

We view our results as the microscopic explanation of the rapid increase of $\Sigma''(0)$ above a certain T within the superconducting state and the related transformation from “gap closing” to “gap filling” behavior of the DOS and the spectral function at large P (and the transformation from gap to Fermi arc behavior at smaller P). To reiterate – we argue that the conventional “gap closing” behavior occurs at $T < T_{c,1}$, while the “gap filling” behavior occurs at $T_{c,1} < T < T_c$, where in Matsubata formalism the pairing is induced by two lowest Matsubata frequencies at which self-energy vanishes, and would not happen if fermions with these two frequencies were eliminated from the gap equation.

The issue which we do not address here is the role of pairing fluctuations. We remind the reader that Eliashberg theory neglects phase and amplitude fluctuations of the pairing vertex and in this respect should be treated as effectively a “mean-field” theory. It is very likely that in some range below Eliashberg T_c fluctuations destroy long-range superconducting order, and the actual $T_{c,act} < T_c$. Our results, that the DOS $N(\omega)$ is non-zero at all ω and the

position of its maximum increases with T , should survive at $T_{c,act} < T < T_c$ as our reasoning only explores the fact that in this T range the feedback from the pairing on the fermionic self-energy is weak. Gap fluctuations reduce this feedback even further. The same holds for the spectral function both at large P and at smaller P . In other words, our theory describes gap filling and Fermi arcs in the pseudogap region. Still, to fully address the issue of gap fluctuations one needs to go beyond Eliashberg theory and analyze the full Luttinger-Ward functional⁵⁹.

The paper is organized as follows. In Sec. II we present the microscopic model of pairing mediated by a gapless boson with $\chi(\Omega_m) = (g/|\Omega_m|)^\gamma$ (the γ -model) and its extension to $N > 1$. We present the set of coupled Eliashberg equations along Matsubara axis for the pairing vertex $\Phi(\omega_m)$ and the fermionic self-energy $\Sigma(\omega_m)$ and summarize, in Sec. II A earlier results of the analysis of the linearized equation for $\Phi(\omega_m)$. At $T = 0$, these results show that there exists the critical N_{cr} , separating the superconducting state at $N < N_{cr}$ and the normal state at $N > N_{cr}$. At $T > 0$, these calculations show that superconductivity emerges for all N , below a certain $T_s(N)$ which only vanishes at $N = \infty$. In Sec. III we discuss the system behavior at $N > N_{cr}$, first in Matsubara frequencies, in Sec. III A, and then in real frequencies, in Sec. III C. We present the analytical solution of the Eliashberg equations at large N and discuss the behavior of the gap, the Free energy and the specific heat, the DOS, and the spectral function. In Sec. IV we discuss system behavior at $N < N_{cr}$, again first in Matsubara frequencies, in Sec. IV A, and then in real frequencies, in Sec. IV B. In Sec. V we summarize our results and compare them with the experimental data.

II. THE MODEL.

We consider a model of itinerant fermions at the onset of a long-range order in either spin or charge channel. At the critical point the propagator of a soft boson becomes massless and mediates singular interaction between fermions. We follow earlier works^{6,7,12–14,16,18,20,21,33,60} and assume that this interaction is attractive in at least one pairing channel and that bosons can be treated as slow modes compared to fermions, i.e., the Eliashberg approximation is valid. Within this approximation one can explicitly integrate over the momentum component perpendicular to the Fermi surface (for a given pairing symmetry) and reduce the pairing problem to a set of coupled integral equations for frequency dependent self-energy $\Sigma(\omega_m)$

and the pairing vertex $\Phi(\omega_m)$ for fermions on the Fermi surface, with effective frequency-dependent dimensionless interaction $\chi(\Omega) = (g/|\Omega|)^\gamma$ (the γ -model, Refs.^{6,7,12,21,33}). This interaction simultaneously gives rise to NFL form of the self-energy in the normal state and to pairing. The equations we analyze are

$$\begin{aligned}\Phi(\omega_m) &= \pi T g^\gamma \sum_{m'} \frac{\Phi(\omega_{m'})}{\sqrt{\tilde{\Sigma}^2(\omega_{m'}) + \Phi^2(\omega_{m'})}} \frac{1}{|\omega_m - \omega_{m'}|^\gamma}, \\ \tilde{\Sigma}(\omega_m) &= \omega_m + g^\gamma \pi T \sum_{m'} \frac{\tilde{\Sigma}(\omega_{m'})}{\sqrt{\tilde{\Sigma}^2(\omega_{m'}) + \Phi^2(\omega_{m'})}} \frac{1}{|\omega_m - \omega_{m'}|^\gamma}\end{aligned}\tag{5}$$

where $\tilde{\Sigma}(\omega_m) = \omega_m + \Sigma(\omega_m)$. Note that we define $\Sigma(\omega_m)$ as a real function of frequency, i.e., without the overall factor of i . The self-energy along Matsubara axis, related by Kramers-Kronig (KK) formula to $\Sigma''(\omega)$ along the real frequency axis, does contain the factor i . The superconducting gap $\Delta(\omega_m)$ is defined as a real variable

$$\Delta(\omega_m) = \omega_m \frac{\Phi(\omega_m)}{\tilde{\Sigma}(\omega_m)}\tag{6}$$

The equation for $\Delta(\omega)$ is readily obtained from (5):

$$\Delta(\omega_m) = \pi T g^\gamma \sum_{m'} \frac{\Delta(\omega_{m'}) - \Delta(\omega_m) \frac{\omega_{m'}}{\omega_m}}{\sqrt{\omega_{m'}^2 + \Delta^2(\omega_{m'})}} \frac{1}{|\omega_m - \omega_{m'}|^\gamma}.\tag{7}$$

This equation contains a single function $\Delta(\omega)$, but for the prize that $\Delta(\omega_m)$ appears on both sides of the equation, which makes (7) less convenient for the analysis than Eqs. (5).

The r.h.s. of the equations for $\Phi(\omega_m)$ and $\Sigma(\omega_m)$ contain divergent pieces from the terms with $m' = m$, i.e., from $\chi(0)$. The divergence can be regularized by moving slightly away from a QCP, in which case $\chi(0)$ is large but finite. This term mimics the effect of non-magnetic impurities. To get rid of the thermal piece in the equations for $\Phi(\omega)$ and $\Sigma(\omega)$, we follow^{36,61} and use the same trick as for the derivation of the Anderson theorem for impurity scattering⁶² Namely, we pull out the term with $m' = m$ from the sum, move it to the l.h.s., and introduce

$$\begin{aligned}\Phi^*(\omega_m) &= \Phi(\omega_m) (1 - Q(\omega_m)), \\ \tilde{\Sigma}^*(\omega_m) &= \tilde{\Sigma}(\omega_m) (1 - Q(\omega_m)) \\ Q(\omega_m) &= \frac{\pi T \chi(0)}{\sqrt{\tilde{\Sigma}^2(\omega_m) + \Phi^2(\omega_m)}}\end{aligned}\tag{8}$$

The ratio $\Phi(\omega_m)/\tilde{\Sigma}(\omega_m) = \Phi^*(\omega_m)/\tilde{\Sigma}^*(\omega_m)$, hence $\Delta(\omega_m)$, defined in (6), is invariant under $\Phi(\omega_m) \rightarrow \Phi^*(\omega_m)$ and $\tilde{\Sigma}(\omega_m) \rightarrow \tilde{\Sigma}^*(\omega_m)$. Using (8), one can easily verify that the equations on $\Phi^*(\omega_m)$ and $\tilde{\Sigma}^*(\omega_m)$ are the same as in (5), but without the thermal piece, i.e., the summation over m' now excludes the divergent term with $m' = m$. The gap function $\Delta(\omega_m)$, defined in (6) is equally expressed in terms of $\Phi^*(\omega_m)$ and $\tilde{\Sigma}^*(\omega_m)$, and the gap equation (7) preserves its form: the sum over m' now excludes the term with $m' = m$, but this term vanishes anyway because the numerator in the r.h.s. of (7) vanishes at $m' = m$. One can also solve (8) backwards and express $\Phi(\omega_m)$ and $\tilde{\Sigma}(\omega_m)$ via $\Phi^*(\omega_m)$ and $\tilde{\Sigma}^*(\omega_m)$ as

$$\begin{aligned}\Phi(\omega_m) &= \Phi^*(\omega_m) (1 + Q^*(\omega_m)), \\ \tilde{\Sigma}(\omega_m) &= \tilde{\Sigma}^*(\omega_m) (1 + Q^*(\omega_m)) \\ Q^*(\omega_m) &= \frac{\pi T \chi(0)}{\sqrt{(\tilde{\Sigma}^*(\omega_m))^2 + (\Phi^*(\omega_m))^2}}\end{aligned}\tag{9}$$

Eq. (5) describes color superconductivity⁹ ($\gamma = 0_+$, $\chi(\Omega_m) \propto \log |\omega_m|$), spin- and charge-mediated pairing in $D = 3 - \epsilon$ dimension^{14,18,20} ($\gamma = O(\epsilon) \ll 1$), a 2D pairing³⁷ with interaction peaked at $2k_F$ ($\gamma = 1/4$), pairing at a 2D nematic/Ising-ferromagnetic QCP^{5,22,63} ($\gamma = 1/3$), pairing at a 2D (π, π) SDW QCP^{6,7,19,64} and an incommensurate CDW QCP^{65,66} ($\gamma = 1/2$), a 2D pairing mediated by an undamped propagating boson ($\gamma = 1$), and the strong coupling limit of phonon-mediated superconductivity¹⁻⁴ ($\gamma = 2$). The pairing models with parameter-dependent γ have also been considered (Refs. 11 and 12). In this communication we consider the set of γ -models with $\gamma < 1$. The analysis for $\gamma > 1$ requires a separate consideration because of the divergence of the normal state self-energy at $T = 0$.

The full set of Eliashberg equations for electron-mediated pairing contains also the equation describing the feedback from the pairing on $\chi(\Omega)$, e.g., the emergence of a propagating mode (often called a resonance mode) in the dynamical spin susceptibility for d -wave pairing mediated by antiferromagnetic spin fluctuations. To avoid additional complications, we do not include this feedback into our consideration. In general terms, the feedback from the pairing makes bosons less incoherent and can be modeled by assuming that γ moves towards $\gamma = 1$ as T moves down from T_c .

The two equations in (5) describe the interplay between two competing tendencies – the tendency towards superconductivity, specified by Φ , and the tendency towards incoherent non-Fermi liquid behavior, specified by Σ . The competition between the two tendencies is encoded in the fact that Σ appears in the denominator of the equation for Φ and Φ appears

in the denominator of the equation for Σ . Accordingly, a large, non-FL self-energy is an obstacle to Cooper pairing, while once Φ develops, it reduces the strength of the self-energy, i.e., moves a system back into a FL regime. Like we said in the Introduction, our goal is to analyze the special role of fermions with Matsubara frequencies $\omega_m = \pm\pi T$ in the situation when the tendency towards pairing is reduced compared to that for NFL normal state. For this, we extend the model to matrix $SU(N)$. Under this extension, the interaction in the particle-hole channel, which gives rise to fermionic self-energy, remains intact, while the interaction in the particle-particle channel acquires an additional factor $1/N$. We emphasize that we extend to $N \neq 1$ *after* we invoke the analog of the Anderson theorem and eliminate the thermal contributions to $\Phi(\omega_m)$ and $\Sigma(\omega_m)$. In this respect our approach differs from the one in Ref.²⁰ There, the extension to large N was done without first subtracting the thermal contributions. As a result, at a finite N there appeared additional terms, singular at a QCP, which gave rise to qualitative changes in the system behavior. In our extension to $N > 1$ these additional terms do not appear. Put it more simply, in our case after the extension the eigenvalues in the pairing channel get multiplied by $1/N$, i.e., a larger magnitude of the original eigenvalue is needed for superconductivity.

The modified equations for $\Phi^*(\omega_m)$ and $\tilde{\Sigma}^*(\omega_m)$ become

$$\begin{aligned}\Phi^*(\omega_m) &= \frac{\pi T}{N} g^\gamma \sum_{m' \neq m} \frac{\Phi^*(\omega_{m'})}{\sqrt{(\tilde{\Sigma}^*(\omega_{m'}))^2 + (\Phi^*(\omega_{m'}))^2}} \frac{1}{|\omega_m - \omega_{m'}|^\gamma}, \\ \tilde{\Sigma}^*(\omega_m) &= \omega_m + g^\gamma \pi T \sum_{m' \neq m} \frac{\tilde{\Sigma}^*(\omega_{m'})}{\sqrt{(\tilde{\Sigma}^*(\omega_{m'}))^2 + (\Phi^*(\omega_{m'}))^2}} \frac{1}{|\omega_m - \omega_{m'}|^\gamma},\end{aligned}\tag{10}$$

and the equation on $\Delta(\omega_m)$ becomes

$$\Delta(\omega_m) = \frac{\pi T}{N} g^\gamma \sum_{m' \neq m} \frac{\Delta(\omega_{m'}) - N \Delta(\omega_m) \frac{\omega_{m'}}{\omega_m}}{\sqrt{\omega_{m'}^2 + \Delta^2(\omega_{m'})}} \frac{1}{|\omega_m - \omega_{m'}|^\gamma}.\tag{11}$$

Below we will also need the expression for the Free energy F_{sc} of a superconductor, described by the Eliashberg theory. The formula for F_{sc} has been obtained in Refs.^{59,67,68} in the studies of phonon-mediated superconductivity ($\gamma = 2$ case at finite ω_D and $N = 1$). Extending the results to $\gamma < 1$, QC regime, and $N \neq 1$, we obtain

$$F_{sc} = -N_0 \left(2\pi T \sum_m \frac{\omega_m^2}{\sqrt{\omega_m^2 + \Delta_m^2}} + \pi^2 T^2 g^\gamma \sum_{m \neq m'} \frac{\omega_m \omega_{m'} + \frac{1}{N} \Delta_m \Delta_{m'}}{\sqrt{\omega_m^2 + \Delta_m^2} \sqrt{\omega_{m'}^2 + \Delta_{m'}^2}} \frac{1}{|\omega_m - \omega_{m'}|^\gamma} \right) \quad (12)$$

where $\Delta_m = \Delta(\omega_m)$. The gap equation (11) is obtained from the condition $\delta F_{sc}/\delta \Delta_n = 0$. In the normal state the expression for the Free energy reduces to

$$F_n = -N_0 \left(2\pi T \sum_m |\omega_m| + \pi^2 T^2 g^\gamma \sum_{m \neq m'} \frac{\text{sgn } \omega_m \text{sgn } \omega_{m'}}{|\omega_m - \omega_{m'}|^\gamma} \right) \quad (13)$$

The difference between F_{sc} and F_n at $T = 0$ is known as the condensation energy of a superconductor. At a finite T ,

$$\begin{aligned} \delta F = F_{sc} - F_n = & -2\pi T N_0 \sum_m |\omega_m| \left(\frac{1}{\sqrt{1 + D_m^2}} - 1 \right) \\ & - N_0 \pi^2 T^2 g^\gamma \sum_{m \neq m'} \frac{\text{sgn } \omega_m \text{sgn } \omega_{m'}}{|\omega_m - \omega_{m'}|^\gamma} \frac{1 + \frac{1}{N} D_m D_{m'} - \sqrt{1 + D_m^2} \sqrt{1 + D_{m'}^2}}{\sqrt{1 + D_m^2} \sqrt{1 + D_{m'}^2}} \end{aligned} \quad (14)$$

where $D_n = D(\omega_n) = \Delta(\omega_n)/\omega_n$. Near $T = T_c$, one can expand δF in powers of Δ_m :

$$\begin{aligned} \delta F = & \pi T N_0 \sum_m |\omega_m| D_m^2 - N_0 \pi^2 T^2 g^\gamma \sum_{m \neq m'} \frac{\text{sgn } \omega_m \text{sgn } \omega_{m'}}{|\omega_m - \omega_{m'}|^\gamma} \left(\frac{1}{N} D_m D_{m'} - \frac{D_m^2 + D_{m'}^2}{2} \right) \\ & + \frac{3}{4} \pi T N_0 \sum_m |\omega_m| D_m^4 - N_0 \pi^2 T^2 g^\gamma \sum_{m \neq m'} \frac{\text{sgn } \omega_m \text{sgn } \omega_{m'}}{|\omega_m - \omega_{m'}|^\gamma} \\ & \times \left(\frac{1}{4} D_m^2 D_{m'}^2 + \frac{3}{8} (D_m^4 + D_{m'}^4) - \frac{1}{2N} D_m D_{m'} (D_m^2 + D_{m'}^2) \right) \end{aligned} \quad (15)$$

A. Linearized gap equation

To obtain T_c it is sufficient to consider the linearized gap equation. It is obtained from (10) by setting Φ^* to be infinitesimally small. Then $\Phi^*(\omega_{m'})$ in the denominators of (10) can be ignored and the self energy $\Sigma^*(\omega_m)$ is approximated by its normal state value. The resulting equations are:

$$\begin{aligned} \Phi^*(\omega_m) &= \frac{g^\gamma}{N} \pi T \sum_{m' \neq m} \frac{\Phi^*(\omega_{m'})}{|\omega_{m'} + \Sigma^*(\omega_{m'})|} \frac{1}{|\omega_m - \omega_{m'}|^\gamma} \\ \Sigma^*(\omega_m) &= g^\gamma \pi T \sum_{m' \neq m} \frac{\text{sgn}(\omega_{m'})}{|\omega_m - \omega_{m'}|^\gamma}. \end{aligned} \quad (16)$$

By power-law counting we expect $\Sigma^*(\omega_m) \propto g^\gamma \omega^{1-\gamma}$. Substituting this into the equation for Φ in (16) we obtain that at $|\omega_{m'}| > |\omega_m|$, the pairing kernel $K = (g^\gamma/N)/(|\omega_{m'}| +$

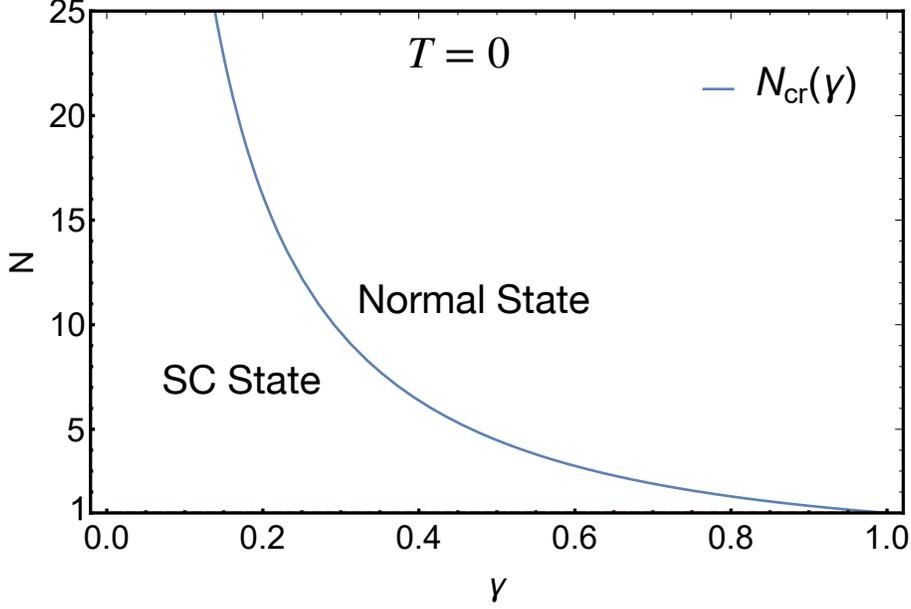


FIG. 7. The behavior of $N_{cr}(\gamma)$, given by Eq. (17). At $T = 0$, this critical N separates superconducting and normal states at $N < N_{cr}(\gamma)$ and $N > N_{cr}(\gamma)$, respectively.

$\Sigma^*(\omega_{m'})/|\omega_{m'}|^\gamma$ is marginal at $|\omega_{m'}| < g$: $K \propto 1/|\omega_{m'}|$ (with prefactor independent on g), and decays as $K \propto g^\gamma/|\omega_{m'}|^{1+\gamma}$ at $|\omega_{m'}| > g$. This implies that T_c , if it exists, should be generally of order g . The marginal form of the kernel is similar to the BCS case and it gives rise to logarithmical growth of the pairing susceptibility within the perturbation theory. However, in distinction to BCS, the marginal form of K holds only if $|\omega_{m'}| > |\omega_m|$, i.e., at each order of perturbation the logarithm is cut by the running frequency in the next cross-section in the Cooper ladder. As the consequence, the summation of the logarithms alone does not lead to the divergence of the pairing susceptibility. In this situation, the conventional wisdom is that the pairing is the threshold phenomenon, i.e., it occurs if the pairing vertex exceeds some finite value. The pairing strength in Eq. (16) is controlled by $1/N$, hence by this logics there should be a critical N_{cr} separating superconducting state at $N < N_{cr}$ and non-superconducting naked critical non-FL state at $N > N_{cr}$. At larger N the tendency towards pairing is stronger than the tendency towards a non-FL behavior; at smaller N the situation is the opposite. The analysis of the pairing problem at $T = 0$ does yield exactly this kind of behavior^{20,21}. Namely, there exists

$$N_{cr} = (1 - \gamma)\Gamma(\gamma/2) \left[\frac{\Gamma(\gamma/2)}{2\Gamma(\gamma)} + \frac{\Gamma(1 - \gamma)}{\Gamma(1 - \gamma/2)} \right], \quad (17)$$

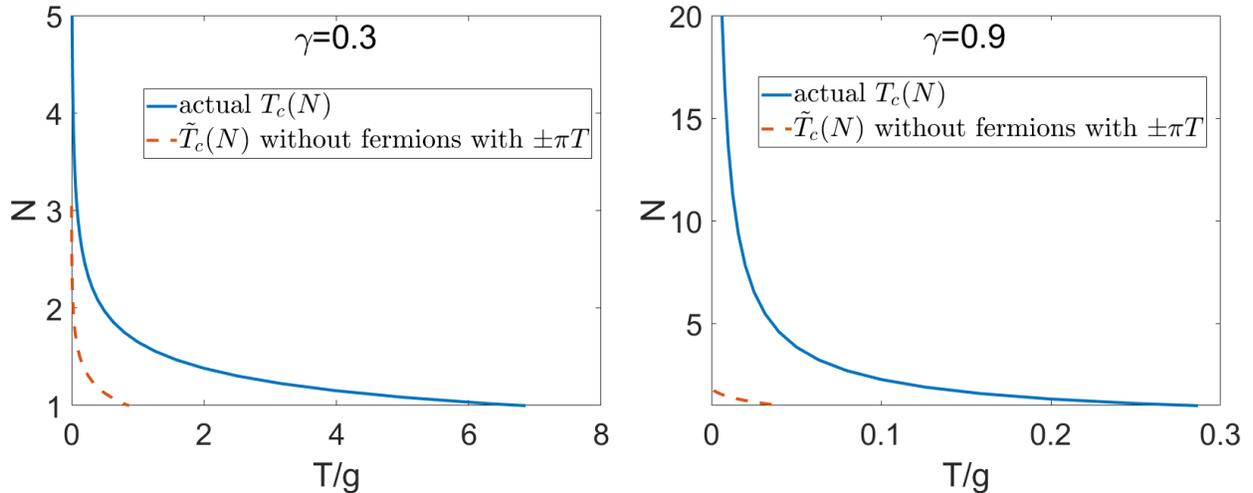


FIG. 8. The pairing instability temperature $T_c(N)$, obtained by solving the linearized gap equation (16) as an eigenvalue/eigengunvction problem for $M = 4000$ Matsubara frequencies, with N playing the role of an eigenvalue. Upper and lower panels are for $\gamma = 0.3$ and $\gamma = 0.9$, respectively. At large N , $T_c(N) \approx (g/2\pi)1/N^{1/\gamma}$. For comparison, we also show $\tilde{T}_c(N)$, which we obtained by solving the linearized gap equation without fermions with Matsubara frequencies $\pm\pi T$. The temperature $\tilde{T}_c(N)$ terminates at $T = 0$ at the critical $N = N_{cr}$.

separating superconducting and non-superconducting states ($\Gamma(\dots)$ is a Gamma function). We plot $N_{cr}(\gamma)$ in Fig.7

The existence of N_{cr} at $T = 0$ would normally imply that this is the termination point of the line $T_c(N)$. However, the numerical solution of (16) yields qualitatively different result: T_c is non-zero at any N , and the line $T_c(N)$ by-passes N_{cr} and approaches zero only at $N \rightarrow \infty$ (see Fig.8). The reason for this behavior has been clarified in Ref.²¹. It turns out that power counting argument that $\Sigma^*(\omega_m) \propto \omega_m^{1-\gamma}$, does not work for the first two Matsubara frequencies $\omega_m = \pm\pi T$, for which Eq. (16) yields $\Sigma^*(\pm\pi T) = 0$. The reason is the presence of the sign-changing factor $\text{sgn}(\omega_{m'})$ in the r.h.s. of the formula for $\Sigma^*(\omega_m)$. For $\omega_m = \pm\pi T$, contributions from positive and negative $\omega_{m'}$ cancel out. To see the consequence of $\Sigma^*(\pm\pi T) = 0$, consider the limit $N \gg 1$ and set external $\omega_m = \pi T$. For $\omega_{m'} = O(T)$, but $\omega_{m'} \neq -\pi T$, the product $\pi T K(\omega_{m'})$ is independent of T and is small in $1/N$. However, for $\omega_{m'} = -\pi T$, this product is $\pi T K = (1/N)(g/(2\pi T))^\gamma$, and it becomes large at small enough

T . A simple experimentation shows that in this situation the gap equation reduces to

$$\begin{aligned}\Phi^*(\pi T) &\approx \frac{1}{N} \left(\frac{g}{2\pi T} \right)^\gamma \Phi^*(-\pi T) \\ \Phi^*(\omega_m) &= \frac{1}{N} \left(\frac{g}{2\pi T} \right)^\gamma \left(\frac{\Phi^*(\pi T)}{|\frac{1}{2} - \frac{\omega_m}{2\pi T}|^\gamma} + \frac{\Phi^*(-\pi T)}{|\frac{1}{2} + \frac{\omega_m}{2\pi T}|^\gamma} \right)\end{aligned}\quad (18)$$

The last equation is for $\omega_m \neq \pm\pi T$. We will be searching for even-frequency solutions of the gap equation: $\Phi^*(\omega_m) = \Phi^*(-\omega_m)$. Then the first equation in (18) sets $T_c = (g/2\pi)1/N^{1/\gamma}$, and the second shows that a non-zero $\Phi^*(\omega_m)$ is induced by $\Phi^*(\pm\pi T)$.

The functional form $T_c \propto 1/N^{1/\gamma}$ at large N has been verified numerically in Ref.²¹ for a particular choice of $\gamma = 0.1$. In Fig.8 we show that the same behavior holds for $\gamma = 0.3$ and 0.9. We now go beyond Ref.²¹ and verify that this behavior of T_c (i.e., that $T_c(N)$ line by-passes N_{cr}) is indeed due to vanishing of the self-energy at the first two Matsubara frequencies. For this, we exclude $\omega_m = \pi T$ from the set of Matsubara frequencies and then solve again the linearized gap equation. The result is shown in Fig.8 We clearly see that \tilde{T}_c , obtained this way, tends to zero above some critical value of N , which numerically is close to $N_{cr}(\gamma)$ in Eq. (17). The outcome is that, without the first two Matsubara frequencies, the system would display a conventional behavior with $\tilde{T}_c(N)$ line terminating at a QCP at $N = N_{cr}$. At larger N , superconductivity would be absent because of stronger tendency towards a (competing) non-FL ground state. That the actual $T_c(N)$ by-passes N_{cr} and vanishes only at $N = \infty$ is then entirely due to the vanishing of the self-energy for fermions with $\omega_m = \pm\pi T$.

The discrepancy between $T_c(N)$ and $\tilde{T}_c(N)$ suggests that physical properties below the actual onset temperature for the pairing $T_c(N)$ depend on whether N is smaller or larger than N_{cr} . When $N > N_{cr}$, the pairing is induced by fermions with $\omega_m = \pm\pi T$ and, the order parameter $\Phi(\omega_m)$ emerges at $T_c(N)$ and vanishes at $T = 0$, i.e., it is non-monotonic as a function of temperature. For $N < N_{cr}$, there are two regimes of qualitatively different behavior – in between $T_c(N)$ and $\tilde{T}_c(N)$, the pairing is induced by fermions with $\omega_m = \pm\pi T$, while at $T < \tilde{T}_c(N)$, fermions with all Matsubara frequencies contribute to the pairing. This last behavior is a conventional one, in the sense that it holds in a non-critical, BCS superconductor, while the behavior at $\tilde{T}_c(N) < T < T_c(N)$ is of non-BCS type as it is due to strong non-FL self-energy at all ω_m except for $\pm\pi T$. At small γ , $N_{cr} \approx 4/\gamma$, and the $T_c(N)$ and $\tilde{T}_c(N)$ lines remain close down to a very small $T \sim g(\gamma)^{1/\gamma} \ll g$. However, for $\gamma \leq 1$, the two lines separate already at $T \leq g$. We note in this regard that the range

between $\tilde{T}_c(N) < T < T_c(N)$ exists for the physical case of $N = 1$, and the lower boundary of this range rapidly decreases as γ approaches the value equal to 1. In other words, even for $N = 1$, there exists an intermediate T range where the pairing is induced by fermions with $\pm\pi T$, and would not exist if these fermions were excluded from the gap equation. The behavior of a system in this intermediate T range at $N = 1$ should be, at least qualitatively, the same as that at large N .

Below we study superconductivity induced by fermions with $\omega_m = \pm\pi T$ in some detail by solving non-linear gap equation at $T < T_c$. We first solve the gap equation in Matsubara frequencies and obtain the gap, the Free energy, and the specific heat, and then convert to real frequencies and obtain the spectral function and the DOS.

III. NON-LINEAR GAP EQUATION, $N > N_{cr}$

We begin with the case $N > N_{cr}$ when $\tilde{T}_c = 0$, i.e. the pairing would be impossible if the self-energy did not vanish at $\omega_m = \pm\pi T$. The limit $N \gg 1$ can be treated analytically and we consider it in some detail below.

A. Non-linear gap equation in Matsubara frequencies.

The non-linear equation for the pairing vertex $\Phi^*(\omega_m)$ along with the equation for the fermionic self-energy $\Sigma^*(\omega_m)$ with the feedback from the pairing are given in (10). We recall that at large N the pairing temperature $T_c(N)$ is obtained by solving the linearized equation for $\Phi^*(\omega_m)$ for fermions with only two Matsubara frequencies $\omega_m = \pm\pi T$; the pairing vertex $\Phi^*(\omega_m)$ for other ω_m is then expressed via $\Phi^*(\pi T) = \Phi^*(-\pi T)$. We assume and then verify that this holds also for $T < T_c$, i.e., that the non-linear gap equation can be approximated by restricting to $\omega_{m'} = \pm\pi T$ in the r.h.s. of Eq. (10). Re-labeling $\Phi^*(\pi T) = \Phi^*(-\pi T) = \Phi_0^*$, $\Sigma^*(\pi T) = -\Sigma^*(-\pi T) = \Sigma_0^*$, and $\tilde{\Sigma}_0^* = \pi T + \Sigma(\pi T)$ to shorten notations, we obtain from (10)

$$\begin{aligned}\Phi_0^* &= \pi T \left(\frac{T_c}{T}\right)^\gamma \frac{\Phi_0}{\sqrt{(\Phi_0^*)^2 + (\tilde{\Sigma}_0^*)^2}} \\ \tilde{\Sigma}_0^* &= \pi T \left[1 + N \left(\frac{T_c}{T}\right)^\gamma \left(1 - \frac{\tilde{\Sigma}_0^*}{\sqrt{(\Phi_0^*)^2 + (\tilde{\Sigma}_0^*)^2}} \right) \right]\end{aligned}\tag{19}$$

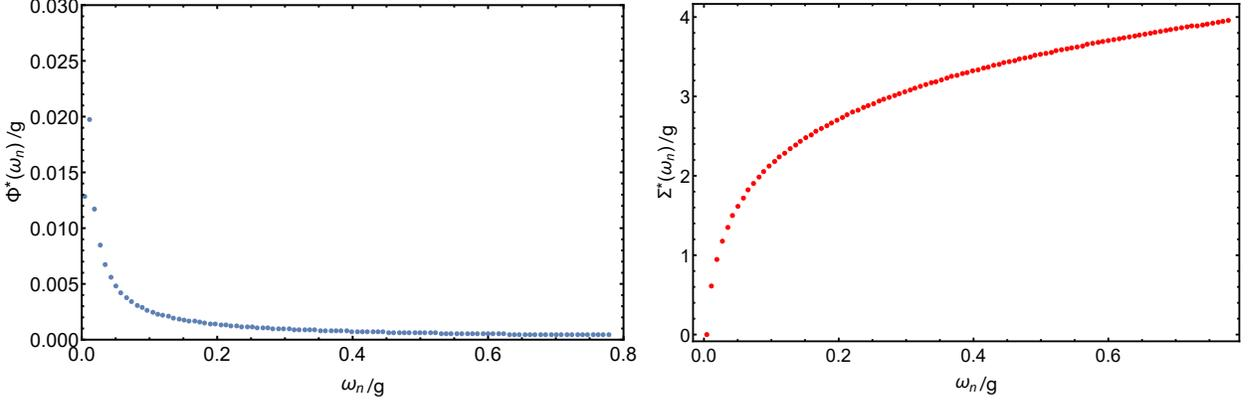


FIG. 9. The pairing vertex $\Phi^*(\omega_m)$ and the self-energy $\Sigma^*(\omega_m)$ from Eq. (22). For definiteness we set $\gamma = 0.9$, $N = 10$, and $T = 0.1T_c$.

The solution of (19) to leading order in $1/N$ is

$$\begin{aligned}\Phi_0^* &= \pi T \left(\frac{2}{N}\right)^{1/2} \left(\frac{T_c}{T}\right)^\gamma \left(1 - \left(\frac{T}{T_c}\right)^\gamma\right)^{1/2} \\ \tilde{\Sigma}_0^* &= \pi T \left(\frac{T_c}{T}\right)^\gamma, \text{ or } \Sigma_0^* = \pi T \left(\left(\frac{T_c}{T}\right)^\gamma - 1\right)\end{aligned}\quad (20)$$

The superconducting gap $\Delta(\pm\pi T) = \Delta_0$ is

$$\Delta_0 = \pi T \left(\frac{2}{N}\right)^{1/2} \left(1 - \left(\frac{T}{T_c}\right)^\gamma\right)^{1/2}\quad (21)$$

The gap Δ_0 vanishes both at $T = 0$ and at $T = T_c$. In between, it is finite, but for any T , $D_0 = \Delta_0/(\pi T)$ is small and at most of order $1/N^{1/2}$. In other words, the gap at $N \gg 1$ remains smaller than the temperature.

Solving next the set of Eliashberg equations for other $\omega_m \neq \pm\pi T$ we obtain at large N

$$\begin{aligned}\Phi^*(\omega_m) &\approx \Phi_0^* \left[\left(\frac{2\pi T}{|\omega_m - \pi T|}\right)^\gamma + \left(\frac{2\pi T}{|\omega_m + \pi T|}\right)^\gamma \right] \\ \Sigma^*(\omega_m) &\approx 2N\tilde{\Sigma}_0^* H\left(\frac{|\omega_m| - \pi T}{2\pi T}, \gamma\right) \text{sgn}\left(m + \frac{1}{2}\right)\end{aligned}\quad (22)$$

where $H(a, b) = \sum_1^a n^{-b}$ is a Harmonic number. We plot $\Phi^*(\omega_m)$ and $\Sigma^*(\omega_m)$ in Fig.9. Note that at $\omega_m \sim T$, $\Sigma^*(\omega_m) \sim N\omega_m$, i.e., $\Sigma^*(\omega_m) \approx \tilde{\Sigma}^*(\omega_m)$.

At large m (but still when $\Sigma^*(\omega_m) \gg \omega_m$)

$$\Phi^*(\omega_m) \approx \frac{2\Phi_0}{|m|^\gamma}, \quad \tilde{\Sigma}^*(\omega_m) \approx 2N \frac{|\tilde{\Sigma}_0|}{1-\gamma} |m|^{1-\gamma} \text{sgn}(m)\quad (23)$$

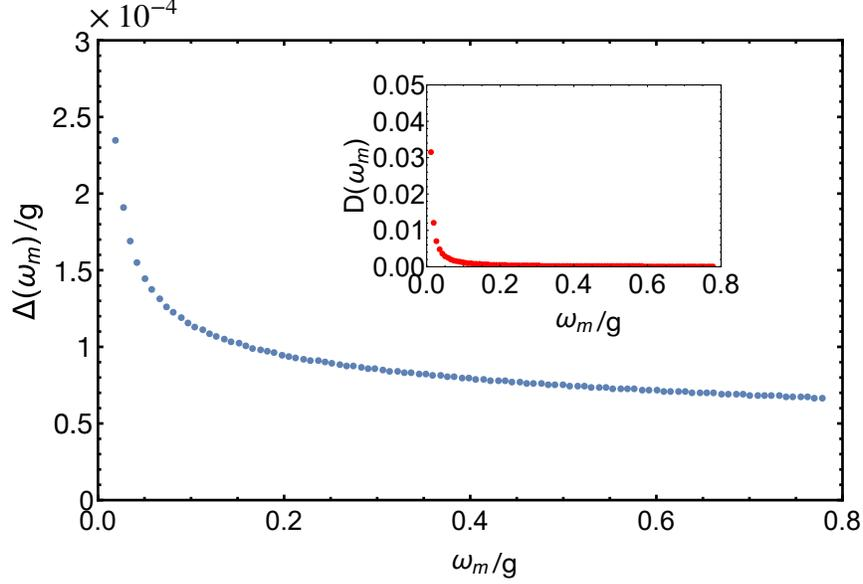


FIG. 10. The pairing gap $\Delta(\omega_m) = \Phi^*(\omega_m)\omega_m/\tilde{\Sigma}(\omega_m)$ and $D(\omega_m) = \Delta(\omega_m)/\omega_m$ for the same parameters as in Fig. 9.

Note that below T_c , the self-energy at all ω_m , including $\omega_m = \pm\pi T$, behaves as $\Sigma^*(\omega_m) \propto T^{1-\gamma}$, consistent with the scaling $\Sigma^*(\omega_m) \propto (\omega_m)^{1-\gamma}$. Still, the self-energy at $\pm\pi T$ is smaller in $1/N$ than $\Sigma^*(\omega_m)$ at other Matsubara frequencies.

From (22) we have

$$\Delta(\omega_m) \sim \frac{\Delta_0}{N} \sim \pi T \left(\frac{2}{N}\right)^{3/2} \left(1 - \left(\frac{T}{T_c}\right)^\gamma\right)^{1/2} \quad (24)$$

both at $m = O(1)$ and at $m \gg 1$. We see that at any $T < T_c$, $\Delta(\omega_m)$ at any Matsubara frequency is parametrically smaller than T . Put it differently, $D(\omega_m) = \Delta(\omega_m)/\omega_m$ is small, of order $1/N^{3/2}$, at $m = O(1)$, and even smaller at larger m . We plot $\Delta(\omega_m)$ and $D(\omega_m)$ in Fig.10.

Taking $-iD_0$ as an estimate for small frequency limit of $D^R(\omega) \equiv \Delta^R(\omega)/\omega$ in real frequencies, we find that $D^R(\omega \rightarrow 0)$ tends to a finite imaginary value, i.e., at large N is a gapless superconductivity in the sense that $\Delta^R(\omega) \propto i\omega$. For notational simplicity for all functions of real frequencies below we will drop the superscript “ R ”.⁶⁹ Using then $N(\omega) = N_0 \text{Re}[1/\sqrt{1 - D^2(\omega)}]$ for the DOS (N_0 is the normal state value), we find that the DOS at zero frequency $N(\omega = 0) = N_0/\sqrt{1 + D_0^2} \approx N_0 \left(1 - \frac{1}{2}D_0^2\right)$ is reduced below T_c compared to the normal state value, but remains finite for any T , like it is expected in a

gapless superconductor.

To verify this result and to get the full form of $N(\omega)$ we need to obtain $\Delta(\omega)$ as a function of a real frequency ω . This is what we will do in Sec. III C. Before that, we use the result for $D(\omega_m)$ and obtain the Free energy $F_{sc}(T)$ and the specific heat $C(T)$ at $N > N_{cr}$.

1. The Free energy and the specific heat

The Free energy F_{sc} and $\Delta F = F_{sc} - F_n$ are given by Eqs. (12)-(15) At large N , we keep only contributions which contain $D_m, D_{m'}$ with $m, m' = 0, -1$. Contributions from D_m with other m are smaller in $1/N$, as we explicitly verified. Using that $\sum_m \frac{\text{sgn } m}{|\pi T \pm \omega_m|^\gamma} = 0$, we obtain from (15)

$$\delta F \approx -2\pi^2 T^2 N_0 \left(\frac{T_c}{T}\right)^\gamma \left[D_0^2 \left(1 - \left(\frac{T}{T_c}\right)^\gamma\right) - \frac{ND_0^4}{4} \right] \quad (25)$$

Varying δF by Δ_0 , one reproduces Eq. (21). Substituting D_0 from (21) into (25), we obtain

$$\delta F \approx -\frac{2}{N}\pi^2 T^2 N_0 \left(\frac{T_c}{T}\right)^\gamma \left(1 - \left(\frac{T}{T_c}\right)^\gamma\right)^2 \quad (26)$$

The specific heat variation between the superconducting and the normal state $\delta C_v = -T\partial^2\delta F/\partial T^2$ is

$$\delta C_v = \frac{2}{N}\pi^2 T_c N_0 C_\gamma \left(\frac{T}{T_c}\right) \quad (27)$$

where

$$C_\gamma(x) = 2\gamma^2 x^{\gamma+1} - 2\gamma(3-\gamma)x(1-x^\gamma) + (2-\gamma)(1-\gamma)x^{1-\gamma}(1-x^\gamma)^2 \quad (28)$$

At $T \rightarrow 0$, $C_\gamma(0) \rightarrow 0$, i.e., δC_v vanishes and C_v recovers its normal state limiting behavior $C_V \propto T^{1-\gamma}$. At $T = T_c - 0$, $C_\gamma = 2\gamma^2$, i.e., the magnitude of the specific heat jump at T_c is

$$\delta C_v = (4\gamma^2/N)\pi^2 T_c N_0. \quad (29)$$

The specific heat in the normal state is obtained from (13). The first term in (13) gives the conventional free-fermion contribution to Free energy $F_{n,free}(T) = F_{n,free}(0) - N_0\pi^2 T^2/3$. The second term gives

$$F_{n,int}(T) = -N_0 N \pi^2 T^2 \left(\frac{T_c}{T}\right)^\gamma \sum_{m \neq m'} \frac{\text{sgn}(m+1/2)\text{sgn}(m'+1/2)}{|m-m'|^\gamma} \quad (30)$$

At $T \sim T_c$, this second term is larger by N than the free-fermion contribution. The calculation of the double sum in (30) requires care as one needs to extract the universal constant on top of formally ultra-violet divergent contribution, which actually is the factor in $F_{n,int}(0)$. To extract the universal constant, we note that the summation over $m - m'$ can be done explicitly. The result is

$$\sum_{m \neq m'} \frac{\text{sgn}(m + 1/2) \text{sgn}(m' + 1/2)}{|m - m'|^\gamma} = 4 \sum_{m=0}^{\infty} H(m, \gamma), \quad (31)$$

where, we remind, $H(m, \gamma) = \sum_1^m 1/p^\gamma$ is the Harmonic number. For the remaining summation we use the Euler-Maclaurin formula

$$\begin{aligned} \sum_{m=0}^{\infty} f(m + 1/2) &= \int_0^{\infty} f(x) dx + Q \\ Q &= - \int_0^{1/2} f(x) dx + \frac{1}{2} f(1/2) - \sum_{n=2}^{\infty} \frac{B_n}{n!} \left. \frac{d^{n-1} f}{dx^{n-1}} \right|_{x=1/2}, \end{aligned} \quad (32)$$

where B_n are Bernoulli numbers. The first term in the upper line in (32) contributes to $F_{n,int}(T = 0)$, the second term determines the universal prefactor in the temperature-dependent piece in the Free energy. It is essential that the argument of the function under the sum is $m + 1/2$ because this is how Matsubara frequency ω_m depends on m . Accordingly, we re-define $H(m + 1/2, \gamma) = \sum_1^{m+1/2-1/2} 1/p^\gamma$ and extend it to a function $H(x, \gamma)$ of a continuous variable x . Evaluating then the integral and the derivatives in the second line in (32) numerically, we obtain

$$\sum_{m=0}^{\infty} H(m, \gamma) = \int_0^{\infty} H(x, \gamma) + Q_\gamma. \quad (33)$$

We plot Q_γ in Fig.11.

Substituting the result into (30) and differentiating the free energy over T , we obtain

$$C_{v,n} = N(4\pi^2 N_0 T_c)(2 - \gamma)(1 - \gamma) Q_\gamma \left(\frac{T}{T_c} \right)^{1-\gamma} \quad (34)$$

The ratio of the specific heat jump to its value at $T = T_c + 0$ is then

$$\frac{\delta C_v}{C_{v,n}} = \frac{1}{N^2} \frac{\gamma^2}{(2 - \gamma)(1 - \gamma) Q_\gamma} \quad (35)$$

We see that the relative jump of C_v at T_c is by $1/N^2$ smaller than in a BCS superconductor. In Fig.12 we plot $C_v(T) = C_{v,n}(T) + \delta C_v(T)$ in the full temperature range below T_c . At sufficiently small T , both C_v and $C_{v,n}$ scales as $T^{1-\gamma}$.

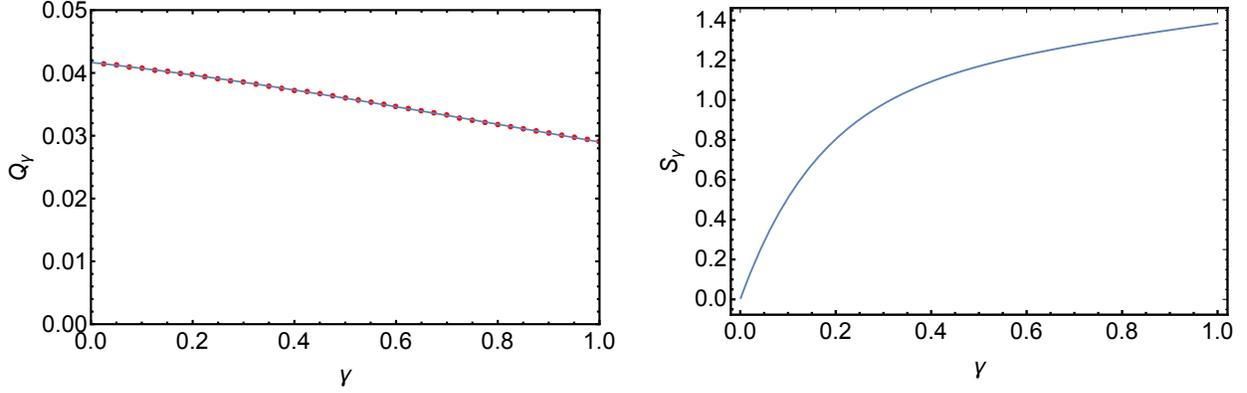


FIG. 11. The plots of the scaling functions Q_γ from Eq. (33) and S_γ from Eq. (52).

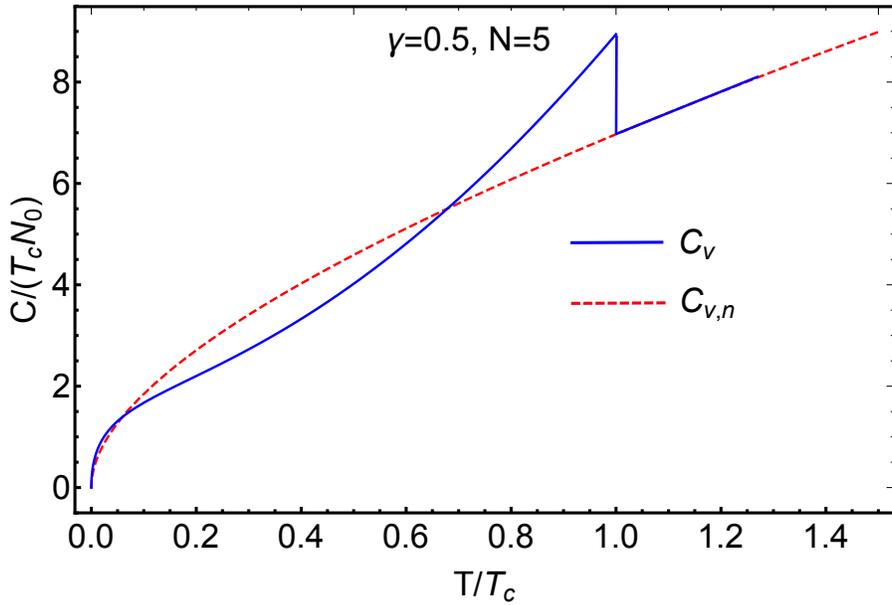


FIG. 12. The specific heat (in units of $T_c N_0$) vs T/T_c . The dashed line is the normal state result. We set $\gamma = 0.5$ and $N = 5$. Observe that the jump of $C(T)$ at T_c is small, and that at low T specific heat returns back to its normal state value.

B. Beyond leading order in $1/N$

We now go beyond the leading order in $1/N$. The goal here is to analyze how fermions with other ω_m affect the magnitudes of $\Phi(\pi T) = \Phi_0$ and $D(\pi T) = D_0$ at a small but finite temperature. We recall that at large N , $\Phi_0 \approx (2/N)^{1/2} \pi T (T_c/T)^\gamma$ and $D_0 \approx (2/N)^{1/2}$. We show that both Φ_0 and D_0 increase as N get smaller.

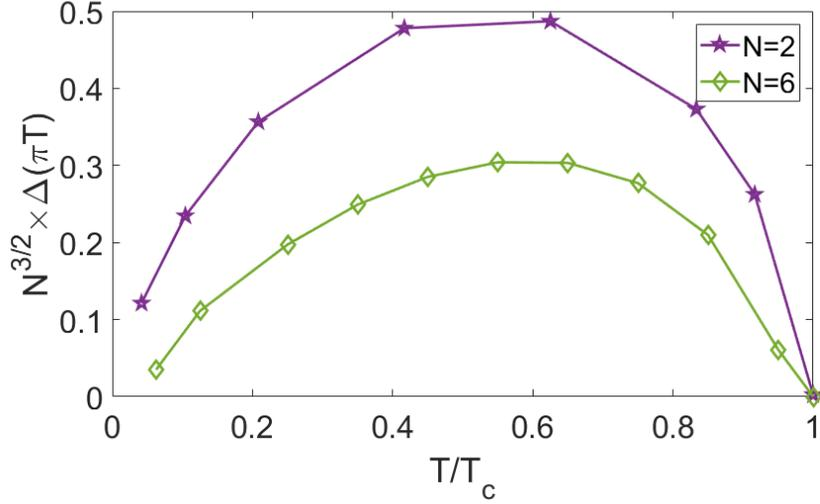


FIG. 13. The gap at the first Matsubara frequency $\Delta(\pi T) = \Delta_0$ as a function of temperature for $\gamma = 0.9$ and two different $N > N_{cr}$. The slope of $\Delta_0(T)$ at small T increases as N gets smaller.

For the analysis to next order in $1/N$ we use the fact that $D_0 \propto 1/N^{1/2}$, while for other Matsubara frequencies $D(\omega_m) \propto 1/N^{3/2}$ (Eqs (21) and (24)). Because D appears in even powers in the equation for the self-energy in (10), the inclusion of these $D(\omega_m)$ with $m \neq 0, -1$ would lead to corrections of at least of order $1/N^2$. To order $O(1/N)$ we then still have the same equation for $\tilde{\Sigma}_0^*$ as in (19). Expanding in this equation in two orders of $D_0^2 \propto 1/N$ and setting $T \ll T_c$, we obtain

$$\tilde{\Sigma}_0^* = N\pi T \left(\frac{T_c}{T}\right)^\gamma \left(\frac{D_0^2}{2} - \frac{3D_0^4}{8}\right) \quad (36)$$

The expansion to next order in $1/N$ in the equation for Φ_0 requires more care as the leading term (the one kept in the first equation in (19)) is of order $1/N^{1/2}$, while other terms in the r.h.s. of the equation for $\Phi^*(\omega_m)$ in (10) are of order $D(\omega_m) \propto 1/N^{3/2}$, i.e., they contain only one additional power of $1/N$. These terms then should be kept in calculation to subleading order in $1/N$. Keeping these terms, we obtain from (10):

$$\begin{aligned} \Phi_0 = & N\pi T \left(\frac{T_c}{T}\right)^\gamma D_0 \left(1 - \frac{D_0^2}{2}\right) \\ & + \sum_{m=1}^{\infty} D(\omega_m) \left(\frac{1}{m^\gamma} + \frac{1}{(m+1)^\gamma}\right) \end{aligned} \quad (37)$$

Substituting $D(\omega_m)$ from Eq. (22):

$$D(\omega_m) = \frac{\Phi^*(\omega_m)}{\tilde{\Sigma}^*(\omega_m)} = \frac{1}{N} \frac{D_0}{H(m, \gamma)} \left(\frac{1}{m^\gamma} + \frac{1}{(m+1)^\gamma} \right) \quad (38)$$

we obtain

$$\Phi_0^* \left(1 - \frac{W_\gamma}{2N} \right) = N\pi T \left(\frac{T_c}{T} \right)^\gamma D_0 \left(1 - \frac{D_0^2}{2} \right) \quad (39)$$

where

$$W_\gamma = \sum_{m=1}^{\infty} \frac{1}{H(m, \gamma)} \left(\frac{1}{m^\gamma} + \frac{1}{(m+1)^\gamma} \right)^2 \quad (40)$$

and, we remind, $H(m, \gamma) = \sum_1^m 1/n^\gamma$ is a Harmonic number. We plot W_γ in inset of Fig.14.

Solving (36) and (39) to order $1/N$ we obtain at low $T \ll T_c$

$$\begin{aligned} \Phi_0^* &= \left(\frac{2}{N} \right)^{1/2} \pi T \left(\frac{T_c}{T} \right)^\gamma \left(1 + \frac{3(W_\gamma - 1)}{4N} \right) \\ \tilde{\Sigma}_0^* &= \pi T \left(\frac{T_c}{T} \right)^\gamma \left(1 + \frac{W_\gamma - 2}{2N} \right) \\ D_0 &= \frac{\Delta_0}{\pi T} \left(\frac{2}{N} \right)^{1/2} \left(1 + \frac{W_\gamma + 1}{4N} \right) \end{aligned} \quad (41)$$

The analysis at larger $T \leq T_c$ proceeds in the same way and we refrain from presenting the full formulas. In Fig. 13 we show $\Delta_0 = \Delta(\pi T)$ as a function of T/T_c for $\gamma = 0.9$ and two different values of $N > N_{cr}$ ($N_{cr} \sim 1.3$ for $\gamma = 0.9$). In both cases, Δ_0 vanishes at $T = 0$, but the slope of $\Delta_0(T)$ at small T gets larger when N decreases.

The result for Φ_0^* can be cast into $\Phi_0^* \approx (2/(N - N_{cr}^*))^{1/2} \pi T \left(\frac{T_c}{T} \right)^\gamma$ where $N_{cr}^* = 3(W_\gamma - 1)/2$ is some γ -dependent constant. Taking this approximate formula as an indication of the evolution of Φ_0^* with decreasing N , we find that $\Phi_0^* \propto T^{1-\gamma}/(N - N_{cr}^*)^{1/2}$. At $N > N_{cr}^*(\gamma)$, Φ_0 vanishes at $T = 0$ (we recall that we consider $\gamma < 1$), but $N = N_{cr}^*(\gamma)$ the slope of $\Phi_0^*(T)/T^{1-\gamma}$ (and of Δ_0) diverges. This divergence is consistent with the $T = 0$ analysis, which indicates that at $N < N_{cr}$, given by Eq. (17), the system has superconducting order at $T = 0$. This will change the system behavior at small temperature and frequencies compared to what we found above. We emphasize that the increase of $\Phi_0^*(T \rightarrow 0)$ is due to the contribution from fermions with $|\omega_m| \neq \pi T$, which give rise to the S term in $1/N$ correction. This means that, as N get reduced, fermions with Matsubara frequencies other than $\pm\pi T$ become progressively more involved in the pairing.

The $N_{cr}^*(\gamma) = 3(W_\gamma - 1)/2$ is an approximate form of critical N and does not have to coincide with the actual $N_{cr}(\gamma)$, given by Eq. (17). We plot both functions in Fig.14. Interestingly, $N_{cr}^*(\gamma)$ and $N_{cr}(\gamma)$ show quite similar variation with γ .

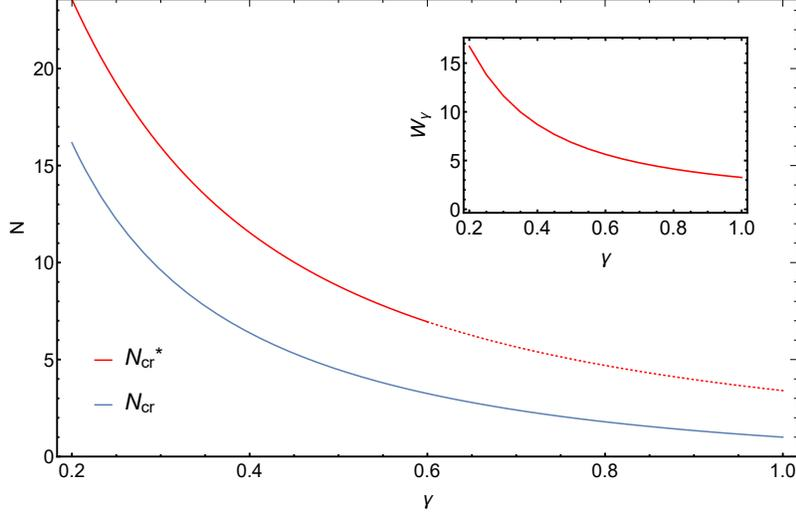


FIG. 14. The approximate $N_{cr}^*(\gamma) = 3(W_\gamma - 1)/2$ vs the actual $N_{cr}(\gamma)$. The inset shows W_γ given by Eq. (40).

We next consider the solutions for the pairing vertex and the self-energy in real frequencies. This will allow us to compute the spectral function $A(\omega)$ and the DOS $N(\omega)$.

C. Non-linear gap equation in real frequencies

The transformation of Elishberg equations for electron-phonon interaction from Matsubara to real frequencies using spectral decomposition method and analytical continuation has been discussed in several publications^{1,3,4}. We extend these results to our case with $\chi(\Omega_m) = (g/|\Omega_m|)^\gamma$. The details of the conversion procedure are presented in the Appendix. The conversion procedure requires special care by two reasons. First, if one simply replaces ω_m by $-i\omega$, the bosonic propagator $\chi(\omega_m + i\omega)$ will have a set of branch cuts in the complex ω plane, along $\omega = i\omega_m + b$, where b is real. One then needs to add additional terms to the r.h.s. of the equations for retarded functions $\Phi(\omega)$ and $\Sigma(\omega)$ to cancel these singularities and restore analyticity. Second, we again need to eliminate singular contributions from the terms with zero bosonic Matsubara frequency. This is done in the same way as in the calculations along the Matsubara axis. Namely, we introduce new functions $\Phi^*(\omega)$ and $\tilde{\Sigma}^*(\omega)$ related to $\Phi(\omega)$ and $\tilde{\Sigma}(\omega) = \omega + \Sigma(\omega)$ as

$$\Phi^*(\omega) = \Phi(\omega) (1 - Q(\omega)), \quad \tilde{\Sigma}^*(\omega) = \tilde{\Sigma}(\omega) (1 - Q(\omega)), \quad (42)$$

where Q_ω is singular (see Eq. (46) below), but $\Phi^*(\omega)$ and $\tilde{\Sigma}^*(\omega)$ are free from singularities. The gap function $\Delta(\omega) = \omega\Phi(\omega)/\tilde{\Sigma}(\omega)$ is equally expressed in terms of $\Phi^*(\omega)$ and $\tilde{\Sigma}^*(\omega)$:

$$\Delta(\omega) = \omega \frac{\Phi(\omega)}{\tilde{\Sigma}(\omega)} = \omega \frac{\Phi^*(\omega)}{\tilde{\Sigma}^*(\omega)} \quad (43)$$

The equations on $\Phi^*(\omega)$ and $\tilde{\Sigma}^*(\omega)$ are the same as on $\Phi(\omega)$ and $\tilde{\Sigma}(\omega)$, but with additional terms which cancel out divergent contribution from $\chi(0)$. We have (see Appendix for details)

$$\begin{aligned} \Phi^*(\omega) &= \frac{\pi T}{N} \sum_m \frac{\Phi^*(\omega_m)}{\sqrt{(\Phi^*(\omega_m))^2 + (\tilde{\Sigma}^*(\omega_m))^2}} \chi(\omega_m + i\omega) \\ &+ \frac{i}{N} \int dx \left[S_\Phi(\omega - x) \chi''(x) (n_F(x - \omega) + n_B(x)) - S_\Phi(\omega) \chi''(x) \frac{T}{x} \right] \\ \tilde{\Sigma}^*(\omega) &= \omega + i\pi T \sum_m \frac{\tilde{\Sigma}^*(\omega_m)}{\sqrt{(\Phi^*(\omega_m))^2 + (\tilde{\Sigma}^*(\omega_m))^2}} \chi(\omega_m + i\omega) \\ &+ i \int dx \left[S_\Sigma(\omega - x) \chi''(x) (n_F(x - \omega) + n_B(x)) - S_\Sigma(\omega) \chi''(x) \frac{T}{x} \right] \end{aligned} \quad (44)$$

where

$$\begin{aligned} S_\Phi(\omega) &= \frac{\Phi(\omega)}{\sqrt{\tilde{\Sigma}^2(\omega) - \Phi^2(\omega)}} = \frac{\Phi(\omega)}{\tilde{\Sigma}(\omega)} \frac{1}{\sqrt{1 - \left(\frac{\Phi(\omega)}{\tilde{\Sigma}(\omega)}\right)^2}} = \frac{\Phi^*(\omega)}{\tilde{\Sigma}^*(\omega)} \frac{1}{\sqrt{1 - \left(\frac{\Phi^*(\omega)}{\tilde{\Sigma}^*(\omega)}\right)^2}} = \frac{\Delta(\omega)}{\sqrt{\omega^2 - (\Delta(\omega))^2}} \\ S_\Sigma(\omega) &= \frac{\tilde{\Sigma}(\omega)}{\sqrt{\tilde{\Sigma}^2(\omega) - \Phi^2(\omega)}} = \frac{1}{\sqrt{1 - \left(\frac{\Phi(\omega)}{\tilde{\Sigma}(\omega)}\right)^2}} = \frac{1}{\sqrt{1 - \left(\frac{\Phi^*(\omega)}{\tilde{\Sigma}^*(\omega)}\right)^2}} = \frac{\omega}{\sqrt{\omega^2 - (\Delta(\omega))^2}} \end{aligned} \quad (45)$$

and $\chi''(x) = \text{sgn}(x) \frac{g^\gamma}{|x|^\gamma} \sin \frac{\pi\gamma}{2}$. In these equations, the solution of the Eliashberg set in Matsubara frequencies, i.e., $\Phi^*(\omega_m)$ and $\tilde{\Sigma}^*(\omega_m)$ are considered as inputs. The first term in each of the two equations is obtained by just replacing ω_m by $-i\omega$, and the second one cancels out non-analyticities. The last piece in the second term cancels out the divergent contribution from $\chi(0)$. Note that the subtraction of the divergence at $x = 0$ has to be done before extending the model to large N . The function $Q(\omega)$, which determines the relations between $\Phi^*(\omega)$ and $\tilde{\Sigma}^*(\omega)$ and the original $\Phi(\omega)$ and $\tilde{\Sigma}(\omega)$, Eqs. (42), is

$$Q(\omega) = \frac{iP}{\sqrt{\tilde{\Sigma}^2(\omega) - \Phi^2(\omega)}} \quad (46)$$

where

$$P = \int dx \chi''(x) \frac{T}{x} = \pi T \chi'(0) \quad (47)$$

Equivalently we can express $\Phi(\omega)$ and $\tilde{\Sigma}(\omega)$ via $\Phi^*(\omega)$ and $\tilde{\Sigma}^*(\omega)$ as

$$\Phi(\omega) = \Phi^*(\omega) (1 + Q^*(\omega)), \quad \tilde{\Sigma}(\omega) = \tilde{\Sigma}^*(\omega) (1 + Q^*(\omega)), \quad (48)$$

where

$$Q^*(\omega) = \frac{iP}{\sqrt{(\tilde{\Sigma}^*)^2(\omega) - (\Phi^*)^2(\omega)}} \quad (49)$$

In Eqs. (45-49) the branch cut of the square root is defined along positive real axis.

At $\omega = 0$ we have

$$\begin{aligned} \Phi^*(0) &= \frac{\pi T}{N} \sum_m \frac{\Phi^*(\omega_m)}{\sqrt{(\Phi^*(\omega_m))^2 + (\tilde{\Sigma}^*(\omega_m))^2}} \chi(\omega_m) + \frac{i}{N} \int dx \chi''(x) \left(\frac{S_\Phi(-x)}{\sinh x/T} - \frac{S_\Phi(0)}{x/T} \right) \\ \tilde{\Sigma}^*(0) &= i\pi T \sum_m \frac{\tilde{\Sigma}^*(\omega_m)}{\sqrt{(\Phi^*(\omega_m))^2 + (\tilde{\Sigma}^*(\omega_m))^2}} \chi(\omega_m) + i \int dx \chi''(x) \left(\frac{S_\Sigma(-x)}{\sinh x/T} - \frac{S_\Sigma(0)}{x/T} \right) \end{aligned} \quad (50)$$

The first term in the formula for $\tilde{\Sigma}^*(0)$ vanishes by symmetry, after summing up the contributions from positive and negative ω_m .

We first consider large N . We assume and then verify that in this case $\tilde{\Sigma}^*$ is parametrically larger than Φ^* not only along the Matsubara axis but also along the real axis. To leading order in $1/N$ we then have for the self-energy

$$\tilde{\Sigma}^*(0) = i \int dx \chi''(x) \left(\frac{1}{\sinh x/T} - \frac{T}{x} \right) = -i\pi T \left(\frac{g}{\pi T} \right)^\gamma S_\gamma \quad (51)$$

where

$$S_\gamma = 2 \sin \pi\gamma/2 \int_0^\infty \frac{dx}{x^\gamma} \left(\frac{1}{\pi x} - \frac{1}{\sinh \pi x} \right) \quad (52)$$

We plot S_γ in Fig.11

For $\Phi^*(0)$ we find from Eq. (50)

$$\Phi^*(0) \approx \frac{\pi T}{N} \sum_m \frac{\Phi^*(\omega_m)}{|\tilde{\Sigma}^*(\omega_m)|} \chi(\omega_m) \quad (53)$$

Using the fact that at large N the dominant contribution to the Matsubara sum comes from $m = 0, -1$ and substituting the expressions for $\Phi^*(\pm\pi T)$ and $\Sigma^*(\pm\pi T)$, we obtain

$$\Phi^*(0) = \left(\frac{2}{N} \right)^{3/2} \pi T \left(\frac{g}{\pi T} \right)^\gamma \left(1 - \left(\frac{T}{T_c} \right)^\gamma \right)^{1/2} \quad (54)$$

Then $D_0 = \Phi^*(0)/\tilde{\Sigma}^*(0)$ is

$$D_0 = i \left(\frac{2}{N} \right)^{3/2} \frac{1}{S_\gamma} \left(1 - \left(\frac{T}{T_c} \right)^\gamma \right)^{1/2} \quad (55)$$

and the DOS at zero frequency is

$$N(0) = N_0 \left(1 - \left(\frac{2}{N} \right)^3 \frac{\left(1 - \left(\frac{T}{T_c} \right)^\gamma \right)}{2S_\gamma^2} \right) \quad (56)$$

This agrees, up to a prefactor, with the result that we obtained along the Matsubara axis, by assuming that $D(\pi T)$ is comparable with $D(\omega = 0)$.

We emphasize that $N(0)$ differs from the normal state value N_0 at all $T < T_c$, including $T = 0$, where we expect superconductivity to disappear. We will show below that the limit $\omega \rightarrow 0$ and $T \rightarrow 0$ has to be taken carefully, and at any non-zero ω the DOS indeed transforms into N_0 at $T \rightarrow 0$. Still, strictly at $\omega = 0$, $N(0) < N_0$. This is similar, but indeed not identical, to behavior of $N(\omega)$ in an ideal BCS superconductor, where $N(0) = 0$ for all T up to T_c , while $N(\omega \neq 0)$ approaches N_0 at $T \rightarrow T_c$.

We next move to finite ω . For $\Phi(\omega)$, the second term in (44) still scales as $\Phi(\omega)/N$ and can be neglected. Evaluating the first term by summing up contributions from $m = 0, -1$ at which $\Phi(\omega_m)/|\tilde{\Sigma}(\omega_m)|$ is the largest at large N , we obtain

$$\Phi^*(\omega) = \left(\frac{2}{N} \right)^{3/2} \pi T \left(\frac{g}{\pi T} \right)^\gamma \left(1 - \left(\frac{T}{T_c} \right)^\gamma \right)^{1/2} F_\Phi \left(\frac{\omega}{\pi T} \right) \quad (57)$$

where

$$F_\Phi(x) = \frac{1}{2} \left(\frac{1}{(1+ix)^\gamma} + \frac{1}{(1-ix)^\gamma} \right) \quad (58)$$

Note that in this large N approximation $\Phi^*(\omega)$ is real and even in ω .

Because $\Phi^*(\omega)$ is small in $1/N^{3/2}$, the self-energy at finite ω remains the same as in the normal state, up to $1/N^3$ corrections:

$$\Sigma^*(\omega) = \pi T \left(\frac{g}{\pi T} \right)^\gamma F_\Sigma \left(\frac{\omega}{\pi T} \right) \quad (59)$$

where

$$F_\Sigma(x) = i \sum_{m=0}^{\infty} \left(\frac{1}{(2m+1+ix)^\gamma} - \frac{1}{(2m+1-ix)^\gamma} \right) - i \sin \frac{\pi\gamma}{2} \int_0^\infty \frac{dy}{y^\gamma} \left(\frac{2}{\pi y} - \coth \frac{\pi y}{2} + \frac{\sinh \pi y}{\cosh \pi y + \cosh \pi x} \right). \quad (60)$$

The first term in $F_\Sigma(x)$ is real, the second is imaginary. At large x (i.e., at $\omega \gg \pi T$), $F_\Sigma(x) \approx (x^{1-\gamma}/(1-\gamma))e^{i\pi\gamma/2}$. We plot the scaling functions $F_\Phi(x)$, $\text{Re}[F_\Sigma(x)]$, and $\text{Im}[F_\Sigma(x)]$ in Fig. 15.

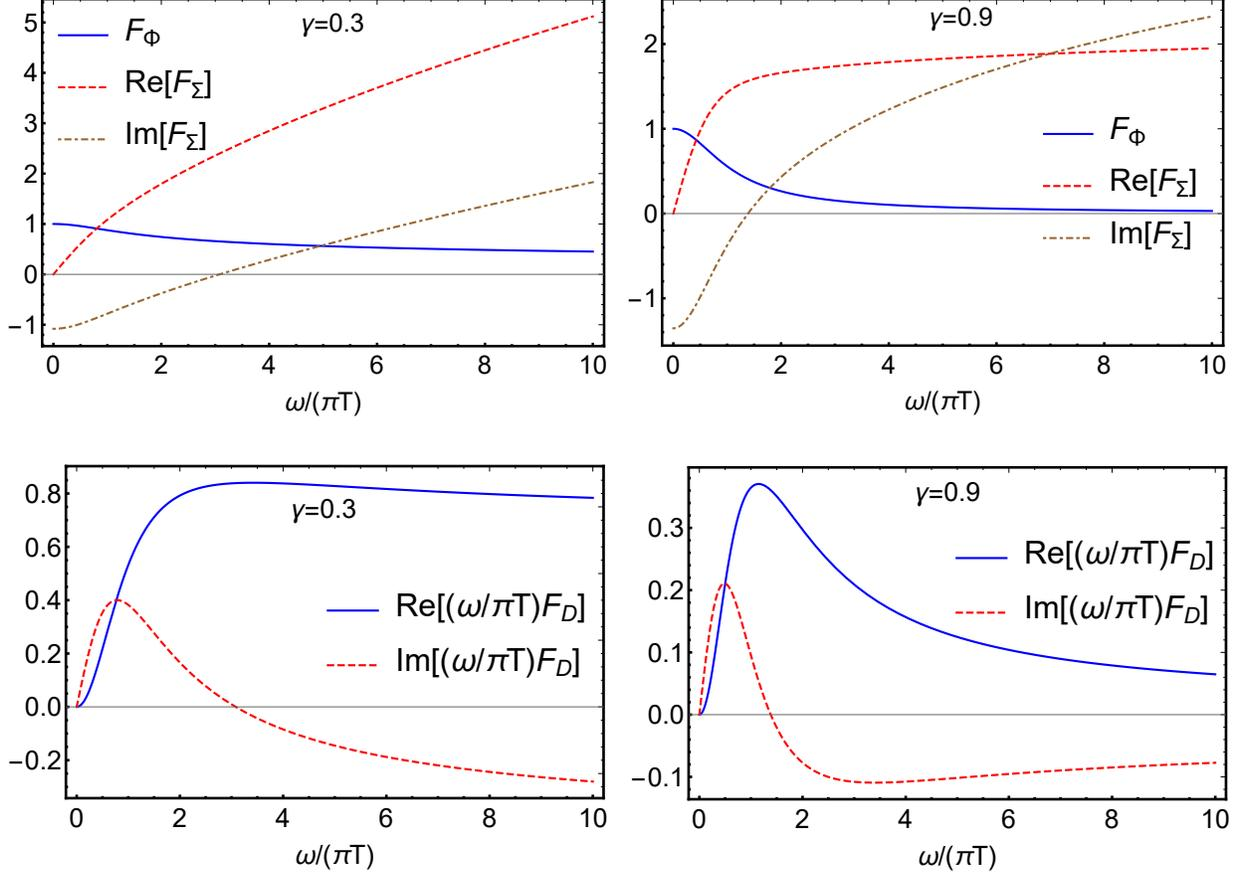


FIG. 15. The scaling functions $F_\Phi(\frac{\omega}{\pi T})$, $F_\Sigma(\frac{\omega}{\pi T})$ and $\frac{\omega}{\pi T}F_D(\frac{\omega}{\pi T}) = \frac{\omega}{\pi T}F_\Phi(\frac{\omega}{\pi T})/F_\Sigma(\frac{\omega}{\pi T})$ for the pairing vertex, the self-energy and the gap function respectively, see Eqs. (58), (60), and (63). We recall that $F_\Phi(\frac{\omega}{\pi T})$ and $F_\Sigma(\frac{\omega}{\pi T})$ are computed without the thermal contribution. The function $F_\Phi(x)$ is real, $F_\Sigma(x)$ and $F_D(x)$ are complex, i.e., the gap function $\Delta(x)$ is a complex function of frequency. The results are for $\gamma = 0.3$ and $\gamma = 0.9$. Observe that $\text{Im} F_\Sigma(x)$ changes sign at some frequency. This sign change is necessary to satisfy KK relation on $\Sigma^*(\pi T) = 0$ (see Fig. 16).

We see that $\text{Im} \left[F_\Sigma \left(\frac{\omega}{\pi T} \right) \right]$ changes sign as a function of frequency (and then $\text{Im} [\Sigma^*(\omega)]$ also changes sign). This sign change is necessary because $\Sigma^*(\pi T) = 0$ and $\text{Im}[\Sigma^*(\omega)]$ are related by Kramers-Kronig(KK) formula,

$$2T \int_0^\infty d\omega \frac{\text{Im} \Sigma^*(\omega)}{\omega^2 + (\pi T)^2} = \Sigma^*(\pi T) = 0, \quad (61)$$

and the vanishing of the integral in (61) is only possible if $\text{Im}[\Sigma^*(\omega)]$ has different sign at small and large frequencies. We verified numerically that the KK relation is indeed satisfied, see

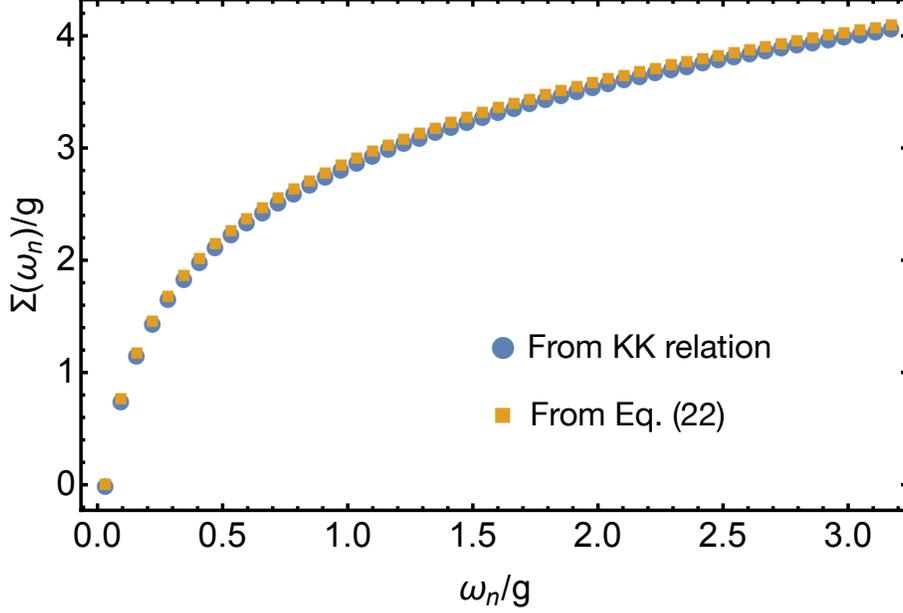


FIG. 16. The verification of the KK transformation. Yellow squares – the self-energy obtained directly along the Matsubara axis: $\Sigma^*(i\omega_n) = 2\pi T(g/2\pi T)^\gamma H(n, \gamma)$, Eq. (22). Blue circles – the self-energy $\Sigma^*(i\omega_n) = -i\pi T(g/\pi T)^\gamma F_\Sigma(\omega_n)$, where $F_\Sigma(i\omega_n) = (2i\omega_n/\pi) \int_0^\infty dx \text{Im} F_\Sigma(x)/(x^2 + \omega_n^2)$ is obtained by KK transformation from $\text{Im} F_\Sigma(x)$ along the real axis, see (60). The two expressions coincide. To better show this we manually split the two expressions for $\Sigma^*(i\omega_n)$ by multiplying the yellow curve by 1.01. Observe that $F_\Sigma(i\pi T) = 0$, i.e., the self-energy $\Sigma^*(i\omega_n)$, extracted from KK transformation, vanishes at the first Matsubara frequency. We set $\gamma = 0.9$ and $T = 0.01g$.

Fig.16. We remind in this regard that Σ^* is the self-energy without the thermal contribution. For the full self-energy $\text{Im}[\Sigma(\omega)]$ indeed remains positive for all frequencies.

Substituting the results for $\Phi^*(\omega)$ and $\tilde{\Sigma}^*(\omega)$ into $D(\omega) = \Phi^*(\omega)/\tilde{\Sigma}^*(\omega)$, we obtain

$$D(\omega) = \left(\frac{2}{N}\right)^{3/2} \left(1 - \left(\frac{T}{T_c}\right)^\gamma\right)^{1/2} F_D\left(\frac{\omega}{\pi T}\right), \quad (62)$$

where at $\omega \leq g$, when the bare ω term is smaller than $\Sigma^*(\omega)$, i.e., $\tilde{\Sigma}^*(\omega) \approx \Sigma^*(\omega)$,

$$F_D(x) = \frac{F_\Phi\left(\frac{\omega}{\pi T}\right)}{F_\Sigma\left(\frac{\omega}{\pi T}\right)} \quad (63)$$

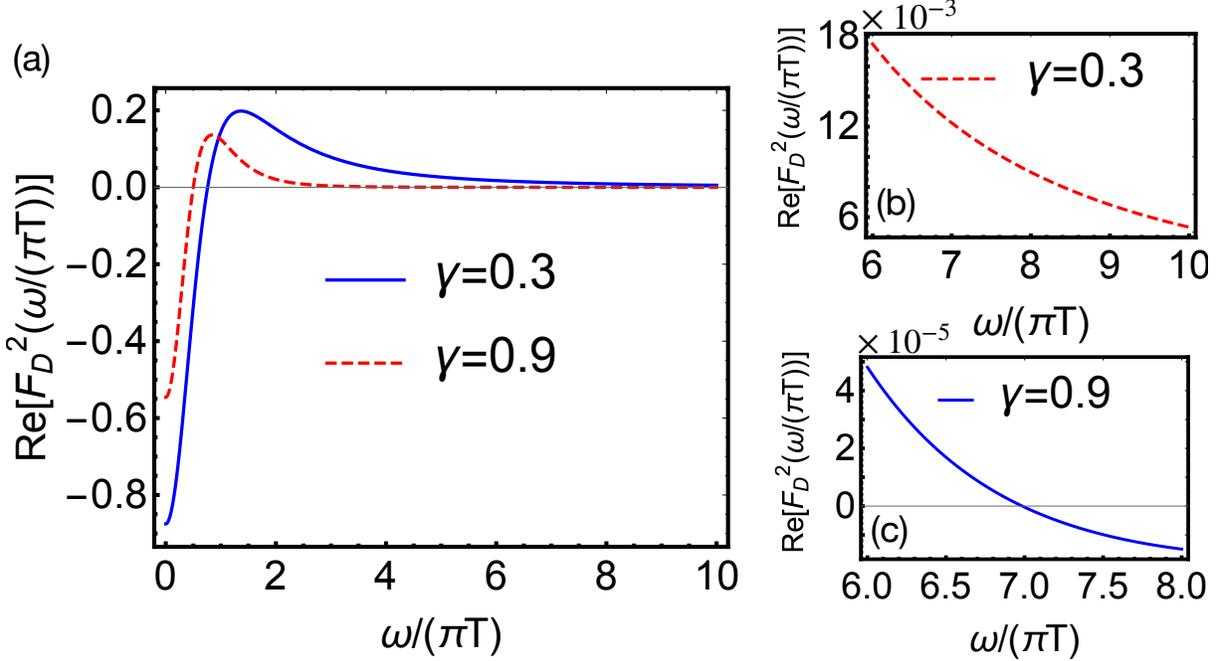


FIG. 17. (a) The real part of the scaling function $F_D^2(\frac{\omega}{\pi T})$, defined in Eq. (63), for $\gamma = 0.3$ and $\gamma = 0.9$. The $\text{Re}[F_D^2(\frac{\omega}{\pi T})]$ determines the frequency dependence of the DOS at large N , Eq. (64). In the normal state $F_D = 0$. Observe that $\text{Re}[F_D^2(\frac{\omega}{\pi T})]$ has a peak at $\omega \sim T$. (b) and (c) The magnified plots of $\text{Re}[F_D^2(\frac{\omega}{\pi T})]$ at larger $\omega/(\pi T)$. For $\gamma = 0.3$, $\text{Re}[F_D^2(\frac{\omega}{\pi T})]$ gradually decreases, for $\gamma = 0.9$ it changes sign at $\frac{\omega}{\pi T} \sim 7$.

The DOS is

$$\begin{aligned}
 N(\omega) &= N_0 \text{Re} \left[\frac{1}{(1 - D^2(\omega))^{1/2}} \right] \approx N_0 \left(1 + \frac{1}{2} \text{Re} [D^2(\omega)] \right) \\
 &= N_0 \left(1 + \frac{1}{2} \left(\frac{2}{N} \right)^3 \left(1 - \left(\frac{T}{T_c} \right)^\gamma \right) \text{Re} \left[F_D^2 \left(\frac{\omega}{\pi T} \right) \right] \right)
 \end{aligned} \tag{64}$$

We see that the magnitude of $N(\omega)/N_0 - 1 = \frac{1}{2} \text{Re} D^2(\omega)$ is determined by the overall temperature-dependent factor in (62) and depends on T/T_c ratio. However, the frequency dependence of $D(\omega)$ and of the DOS is determined by $F_D(\omega/(\pi T))$, which for any given γ is a universal function of ω/T and does not depend on T/T_c . This implies that the characteristic frequency, at which $N(\omega)$ deviates from N_0 , is determined by the temperature rather than by the magnitude of the superconducting gap, as was the case for a BCS superconductor.

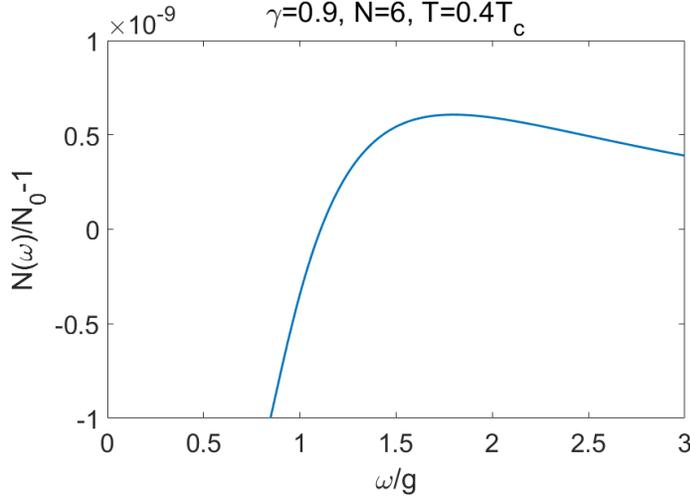


FIG. 18. DOS at large $\omega \sim g$ for $\gamma = 0.9$. We set $N = 6$ and $T = 0.4T_c$. At some $\omega \sim g$, $N(\omega) - N_0$ changes sign from negative to positive, and at even larger frequencies approaches zero from above.

Because $F_\Phi(x)$ is real,

$$\text{Re } F_D^2(x) = F_\Phi^2(x) \frac{(\text{Re } F_\Sigma(x))^2 - (\text{Im } F_\Sigma(x))^2}{((\text{Re } F_\Sigma(x))^2 + (\text{Im } F_\Sigma(x))^2)^2} \quad (65)$$

At small $x = \omega/\pi T$, $\text{Re } F_\Sigma(x) \propto x^2$ and $\text{Im } F_\Sigma(x)$ is finite. Then $\text{Re } F_D^2(x)$ is negative. At x where $\text{Im } F_\Sigma(x)$ changes sign, $\text{Re } F_\Sigma(x)$ is finite, hence for this x , $\text{Re } F_D^2(x)$ is positive. In between $\text{Re } F_D^2(x)$ then necessarily changes sign. This in turn implies that $N(\omega) < N_0$ at small x and exceeds N_0 at larger x . At even larger $x \gg 1$, $N(\omega)$ approaches N_0 . Then, for any γ , $N(\omega)$ has a dip at $\omega = 0$ and a hump at a characteristic frequency set by temperature, rather than by the gap itself. This frequency then *increases with increasing T* , in qualitative difference with a BCS superconductor, in which the maximum in the DOS is located at $\omega = \Delta(T)$, and shifts to a lower frequency with increasing T because $\Delta(T)$ gets smaller. We plot $\text{Re } F_D^2(x)$ in Fig.17 for two different γ . The hump at $\omega \sim T$ is clearly visible. The position of the hump shifts to a lower frequency with increasing γ but remains at a finite ω even at $\gamma = 1$.

On a more careful look, we find that there is still a small difference in the behavior of the DOS between $\gamma < 1/2$ and $\gamma > 1/2$. Namely, at $\omega \gg T$, $\text{Re } \Sigma^*(x) = \cos \pi\gamma/2(x^{1-\gamma}/(1-\gamma))$ and $\text{Im } \Sigma^*(x) = \sin \pi\gamma/2(x^{1-\gamma}/(1-\gamma))$. As a result, $\text{Re } F_D^2(x) \propto \cos \pi\gamma$, i.e., it is positive at $\gamma < 1/2$ and negative at $\gamma > 1/2$. This implies that for $\gamma > 1/2$ $N(\omega)$ crosses N_0 twice at $\omega = O(T)$ because $(\text{Im } F_\Sigma(x))^2$ is larger than $(\text{Re } F_\Sigma(x))^2$ at both large and small

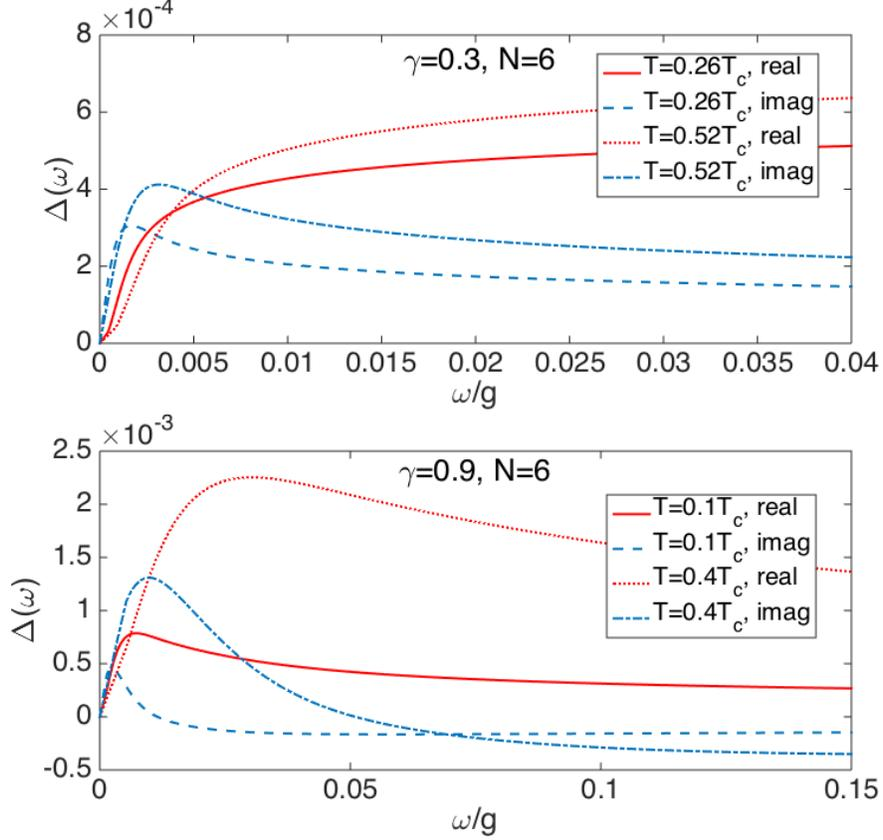


FIG. 19. $\Delta(\omega)$ for various $T > T_{cross}$. Upper panel: $\gamma = 0.3, N = 6$. Lower panel: $\gamma = 0.9, N = 6$. Red lines are for the real part $\Delta'(\omega)$ and blue lines are for the imaginary part $\Delta''(\omega)$. At small but non zero ω , both the real and imaginary parts are finite, in contrast to the BCS-like behavior where $\Delta''(\omega)$ is zero up to some $\omega_0 \approx \Delta'$ at low temperatures.

frequencies. The second crossing at $x \sim 7$ is seen in Fig. 15 for $\gamma = 0.9$. Digging further into this issue, we find that for $\gamma > 1/2$, $N(\omega)$ crosses N_0 one more time, now at $\omega \sim g \gg T$, when the bare ω term in $\tilde{\Sigma}^*(\omega)$ becomes relevant, and at highest ω approaches N_0 from above. To see this, we extend the analysis of the DOS to $\omega \sim g$. The calculation is straightforward and we only cite the result: the difference $N(\omega)/N_0 - 1$ at $\omega \sim g$ is proportional to $\cos \pi\gamma + (1-\gamma)^2(\omega/g)^{2\gamma} + 2(1-\gamma)(\omega/g)^\gamma \cos \pi\gamma/2 = 0$. Solving this equation for $\gamma > 1/2$, we find the sign change of $N(\omega)/N_0 - 1$ at $\omega = \omega_1 \sim g$. We show this in Fig. 18.

In Fig.19 and Fig.20 we show the results of the full numerical calculation of the temperature evaluation of the gap $\Delta(\omega)$ and the DOS $N(\omega)$ for two values of γ : $\gamma = 0.3$ and

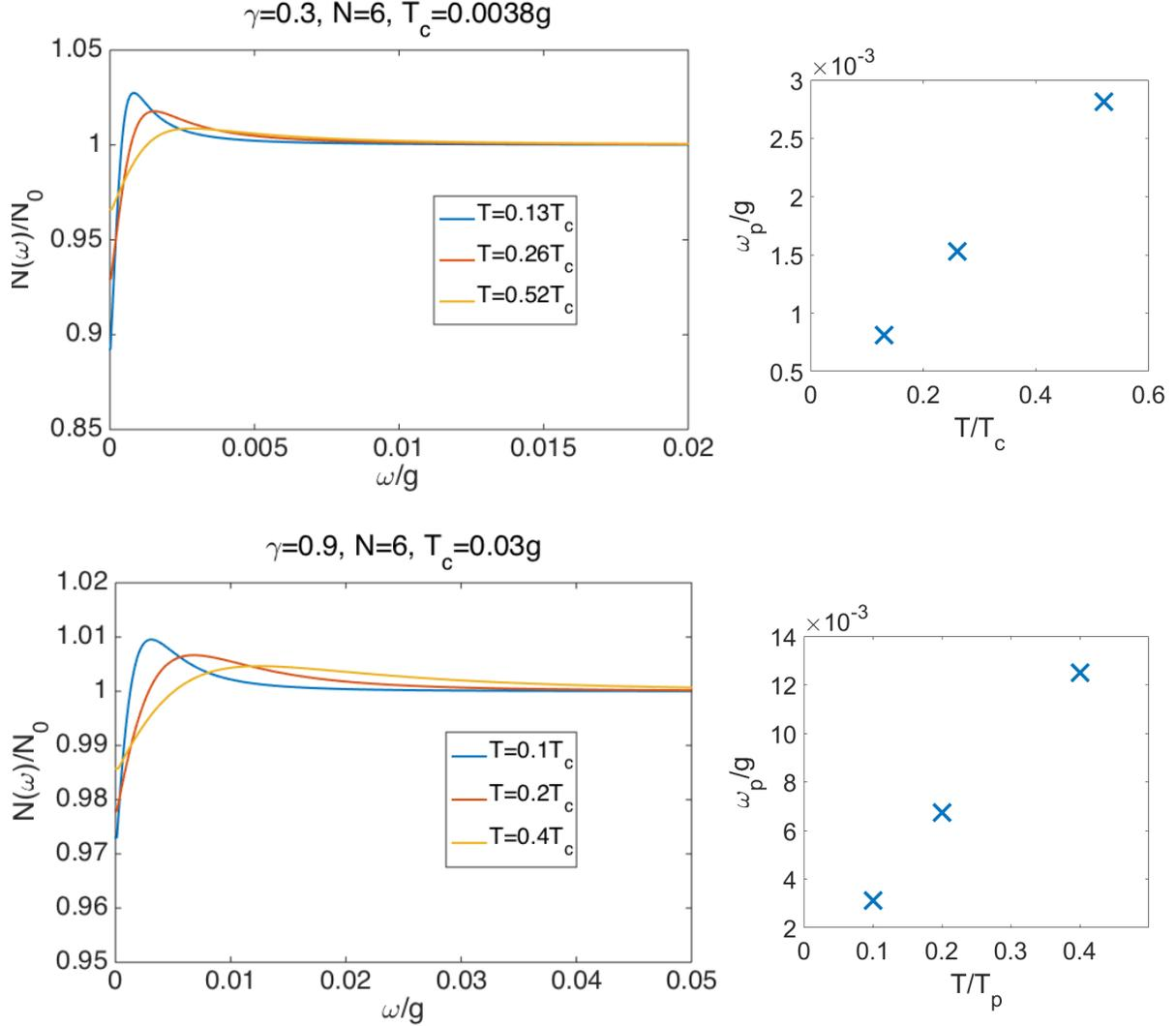


FIG. 20. The DOS $N(\omega)$ for various $T > T_{cross}$. Upper panel: $\gamma = 0.3, N = 6$. Lower panel: $\gamma = 0.9, N = 6$. Right panels: The temperature dependence of the characteristic frequency ω_p , defined as the peak position of the $N(\omega)$.

$\gamma = 0.9$. For $\gamma = 0.9, N = 6$ is above $N_{cr} \sim 1.3$. For $\gamma = 0.3$ we show the results for $N = 6$, which is below $N_{cr} \approx 9.6$ (the numerical analysis for $N > N_{cr}$ for such small γ is challenging). For $N < N_{cr}$, the behavior similar to the one at large N exists above the crossover temperature $T_{cross}(N)$ (see Sec. IV) and we show the results only in this T range. The value of $T_{cross}(N = 6)$ for $\gamma = 0.3$ is only $0.01T_c$, so the range of $T > T_{cross}$ is rather wide. The gap $\Delta(\omega)$ is complex even at very small ω , in contrast to the conventional BCS-like behavior where $\Delta(\omega)$ is almost real up to some frequency which is approximately equal to this real

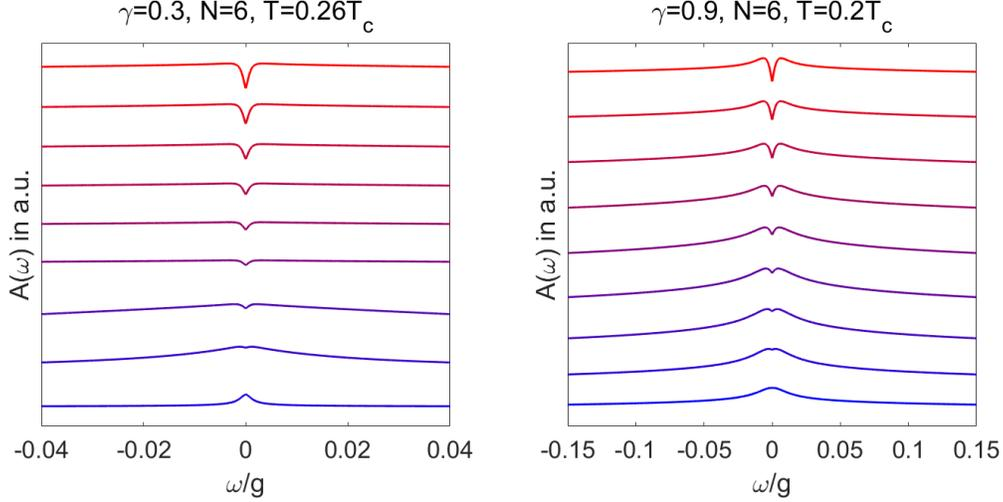


FIG. 21. The spectral function $A(\omega)$ at a fixed $T > T_{cross}$, plotted as a function of ω for various values of parameter P , which measures the strength of thermal contributions to the self-energy and the pairing vertex. At large P , $A(\omega)$ shows the same behavior as the DOS, with the dip at small ω . At small P , it shows instead the maximum at $\omega = 0$. The plots are for $\gamma = 0.3$ and $\gamma = 0.9$.

value. For the DOS we clearly see that there is a dip in $N(\omega)$ at small frequencies and a characteristic frequency ω_p at which $N(\omega)$ approaches N_0 is set by the temperature.

A remark is in order here. The $\int d\omega N(\omega)$, with $N(\omega)$ as in Fig.20 does have some T dependence. At a first glance, this contradicts the requirement that the total number of particles is a conserved quantity. In fact, there is no contradiction. The reasoning is that the momentum integration in Eliashberg equations is performed assuming particle-hole symmetry, i.e., neglecting contributions from energies of order μ . There are additional contributions to the DOS from energies of order μ , both in the normal and the superconducting state. They are not equal, because μ changes between normal and superconducting states⁷⁰. This additional contribution must be included to ensure particle conservation.

We next consider the spectral function $A(\omega) = -(1/\pi) \text{Im}[G(k_F, \omega)]$. In terms of original $\Phi(\omega)$ and $\tilde{\Sigma}(\omega)$, we have

$$A(\omega) = -\frac{1}{\pi} \text{Im} \left[\frac{\tilde{\Sigma}(\omega)}{\tilde{\Sigma}^2(\omega) - \Phi^2(\omega)} \right] \quad (66)$$

Expressing $\tilde{\Sigma}(\omega)$ and $\Phi(\omega)$ via $\tilde{\Sigma}^*(\omega)$ and $\Phi^*(\omega)$, Eq. (49), we find

$$A(\omega) = -\frac{1}{\pi} \text{Im} \left[\frac{\tilde{\Sigma}^*(\omega)}{(\tilde{\Sigma}^*(\omega))^2 - (\Phi^*(\omega))^2} L(\omega) \right] \quad (67)$$

where

$$L(\omega) = \frac{1}{1 + Q^*(\omega)} = \frac{\sqrt{\tilde{\Sigma}^*(\omega)^2 - \Phi^*(\omega)^2}}{iP + \sqrt{\tilde{\Sigma}^*(\omega)^2 - \Phi^*(\omega)^2}} \quad (68)$$

To leading order in $1/P$, $A(\omega) \propto \frac{1}{P} \text{Re} \left[\frac{1}{\sqrt{1 - (\Phi^*(\omega)/\tilde{\Sigma}^*(\omega))^2}} \right] \propto N(\omega)/N_0$, i.e., the spectral function has the same dependence on ω as the DOS. Accordingly, at a finite T , $A(\omega)$ is non-zero for any frequency, and the position of the maximum in $A(\omega)$ scales with T and remains at a finite frequency at T_c (Fig.21). Like we said, this behavior has been termed as “gap filling”. If P is finite, either because the system is at some distance from a QCP, or we probe $A(\omega)$ for fermions not connected by momenta at which static χ diverges (like near-nodal fermions in the cuprates, if a pairing boson is an antiferromagnetic spin fluctuation), the behavior of $A(\omega)$ depends on the interplay between P and the other term in $L(\omega)$ in (68). If P is smaller, $A(\omega)$ is given by (67), (68). Substituting the expressions for $\Phi^*(\omega)$ and $\tilde{\Sigma}^*(\omega)$ we find that in this situation $A(\omega)$ is peaked at zero frequency, as if the system was in the normal state (see Fig.21).

The analysis beyond the leading order in $1/N$ proceeds in the same way as for Matsubara frequencies. As N gets smaller, the maximum in the DOS becomes more pronounced, and, at the same time, the DOS at zero frequency, $N(0)$ gets smaller. These modifications get larger as N decreases towards N_{cr} and eventually qualitatively change the system behavior at $N < N_{cr}$ and $T < T_{cross}$, as we show in the next Section.

IV. THE CASE $N < N_{cr}$

At smaller $N < N_{cr}$ analytical solution is difficult to obtain because there is no obvious small parameter, so our discussion will be based on numerical results.

A. Non-linear gap equation in Matsubara frequencies

In Fig.22 we show the results for $\Phi^*(\omega_m)$ and $\Delta(\omega_m)$. We see that now $\Phi^*(\pi T) = \Phi_0^*$ and $\Delta(\pi T) = \Delta_0$ tend to finite values at $T \rightarrow 0$, i.e., show a “conventional” superconducting behavior. Because at $T = 0$ Matsubara frequency is a continuous variable, and it does not select between $\pm\pi T$ and other frequencies, the development of a finite gap at $T = 0$ implies that at $N < N_{cr}$ and a finite T , there should exist a T range in which all Matsubara

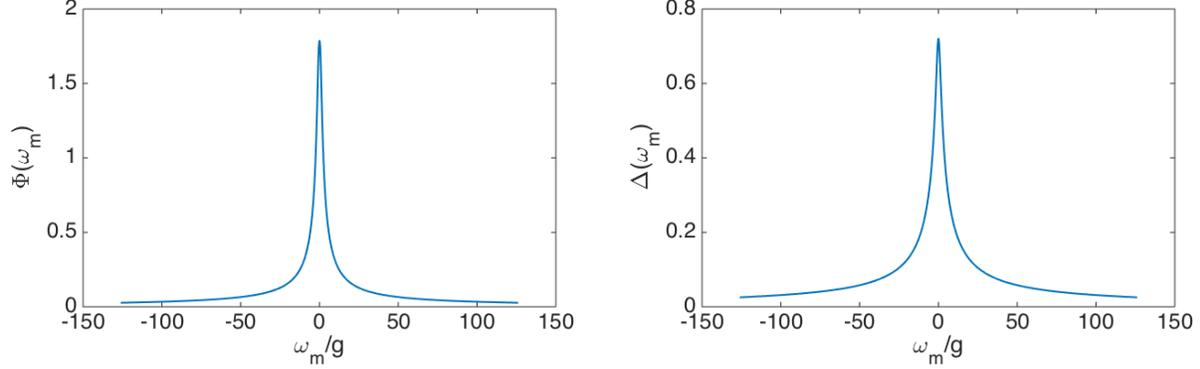


FIG. 22. The pairing vertex $\Phi(\omega_m)$ and the gap $\Delta(\omega_m)$ as functions of Matsubara frequency for $\gamma = 0.9$, $N = 1$, and $T = 0.18T_c < T_{cross}$.

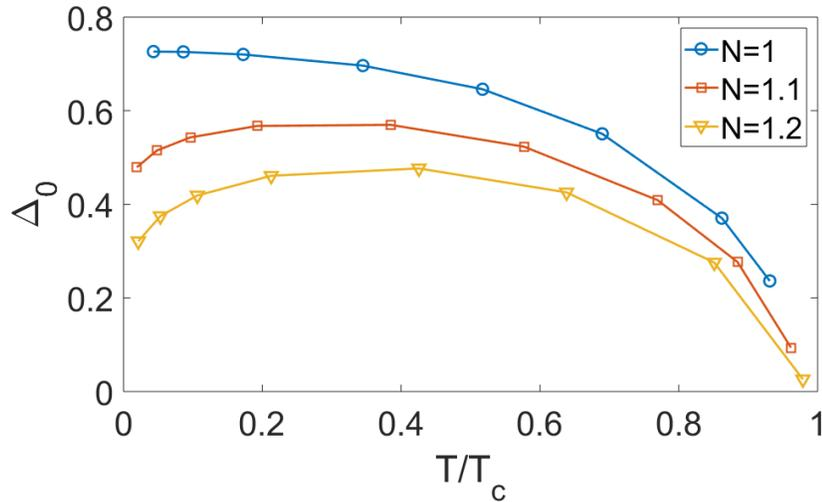


FIG. 23. The gap $\Delta(\pi T) = \Delta_0$ as a function of temperature for $\gamma = 0.9$ and three different $N < N_{cr} \approx 1.34$. The gap now tends to a finite value at $T = 0$. For N slightly below N_{cr} , $\Delta_0(T)$ is still non-monotonic, but for $N = 1$, Δ_0 monotonically increases with decreasing T .

frequencies equally contribute to the pairing, i.e., fermions with $\omega_m = \pm\pi T$ are no longer crucial to the pairing. This is consistent with our earlier result that at $N < N_{cr}$, the transition temperature remains finite even we exclude fermions with $\omega_m = \pm\pi T$ from Eliashberg equations ($\tilde{T}_c(N)$ in Fig.8).

In Fig.23 we show $\Delta(\pi T) = \Delta_0$ as a function of T . The temperature dependence of Δ_0 is still non-monotonic, i.e., as T is reduced below T_c , Δ_0 first increases, and then drops

below a certain T , before reaching a finite value at $T \rightarrow 0$. As $N \rightarrow 1$, the maximum in $\Delta_0(T)$ becomes shallow. The frequency dependence of $\Phi^*(\omega_m)$ and of $\Delta(\omega_m)$ at a given T is monotonic, with the maximum at $|\omega_m| = \pi T$.

In Fig.23 we compare the behavior of $\Delta_0(T)$ at $N > N_{cr}$ and $N < N_{cr}$. Near T_c , the behavior in the two cases is the same, but at low T $\Delta_0(T)$ at $N > N_{cr}$ continue decreasing, while $\Delta_0(T)$ at $N < N_{cr}$ saturates. The temperature at which the two curve separate marks the crossover between the conventional behavior at low T and the behavior, undistinguishable from the one at $N > N_{cr}$, at higher T . In the higher T region, the pairing can still be viewed as induced by fermions with Matsubara frequencies $\pm\pi T$. The crossover line $T_{cross}(N)$ ends at $T = 0$ at $N = N_{cr}$, just like $\tilde{T}_c(N)$, but these two temperatures are not directly proportional to each other.

B. Non-linear gap equation in real frequencies

We used the same computational procedure as at large N and obtained $\Phi^*(\omega)$, $\tilde{\Sigma}^*(\omega)$, and $\Delta(\omega)$ along the real frequency axis. We present the results in Fig.24. We again see the crossover in the system behavior around $T_{cross}(N)$. At smaller T , the behavior of the gap function is conventional in the sense that $\Delta'(\omega = 0)$ is finite and $\Delta''(\omega)$ emerges only above a finite frequency $\omega_0 \approx \Delta'(0)$. At higher T , at small frequencies $\Delta''(\omega) \propto \omega$ and $\Delta'(\omega) \propto \omega^2$, i.e., the systems displays gapless superconductivity. The self-energy $\Sigma^*(\omega)$ is strongly reduced below ω_0 at small T compared to that in the normal state, but almost recovers the normal state value in the regime of gapless superconductivity (Fig.24).

In Fig.25 we show the behavior of the DOS $N(\omega)$. We see qualitative change of the behavior between $T > T_{cross}(N)$ and $T < T_{cross}(N)$. At smaller T , the DOS is similar to that in a BCS superconductor: it has a sharp peak at $\omega \approx \Delta(0)$ and nearly vanishes below the peak frequency. At T increases but remains smaller than $T_{cross}(N)$, the position of the maximum in $N(\omega)$ moves to a smaller frequency because $\Delta(0)$ get reduced, i.e., the gap in the DOS “closes in”. However, at higher $T > T_{cross}(N)$, the DOS becomes non-zero at all frequencies, and the position of its maximum moves to a higher frequency and remains finite at $T = T_c - 0$, i.e., the gap in the DOS “fills in”. We plot the variation of the position of the maximum in $N(\omega)$ with T on the right side of each DOS in Fig.25.

The spectral function $A(\omega)$ shows the similar crossover (Fig.26). In the limit when

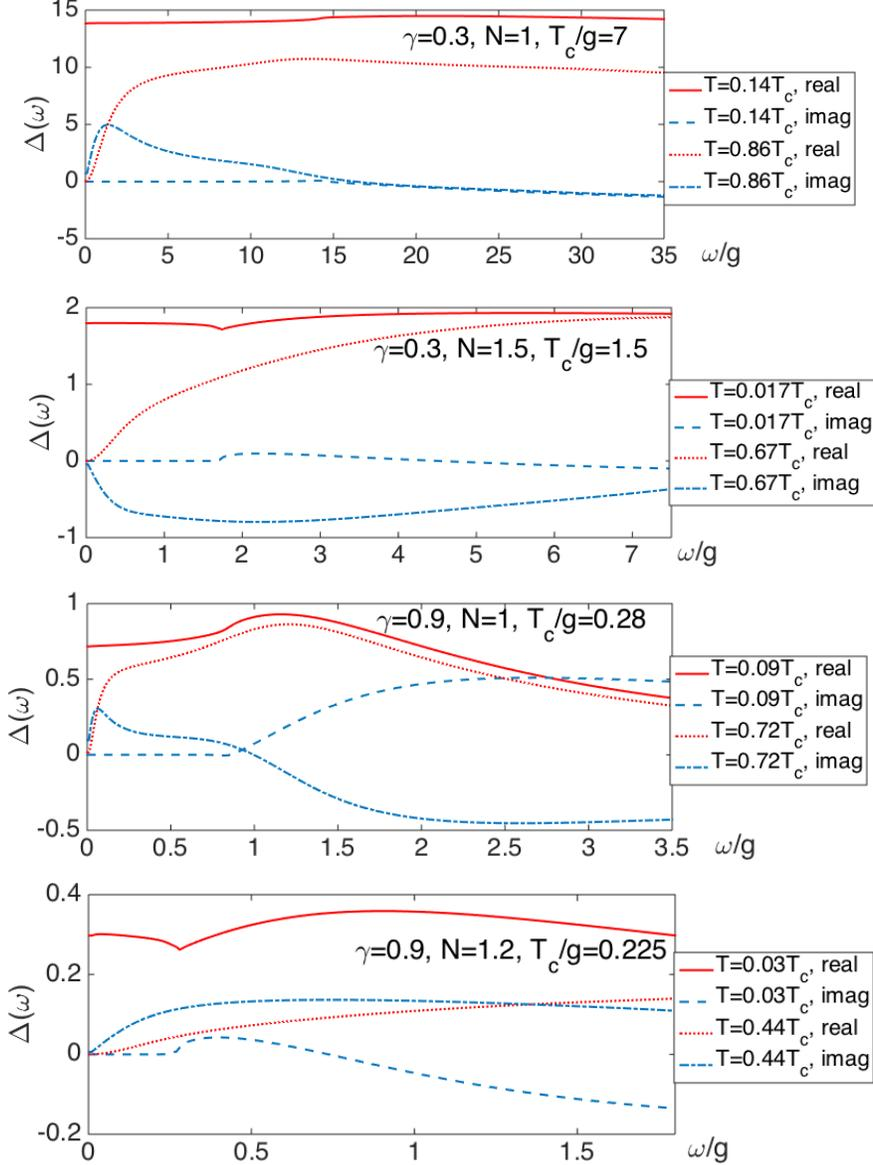


FIG. 24. Real and imaginary parts of the gap $\Delta(\omega)$ as functions of ω for various T . The results are for $\gamma = 0.3$ and $\gamma = 0.9$, in both cases for $N < N_{cr}$. Red and blue lines are for $\Delta'(\omega)$ and $\Delta''(\omega)$, respectively. The data clearly show a crossover at $T \sim T_{cross}$ from BCS-like behavior at smaller T to the behavior similar to that at $N > N_{cr}$, at larger T .

the thermal contribution is large, it shows the same behavior as $N(\omega)$. In the opposite limit, $A(\omega)$ at $T < T_{cross}(N)$ has two sharp peaks at frequencies close to $\pm\Delta(0)$, and at $T > T_{cross}(N)$ it has a single peak at $\omega = 0$

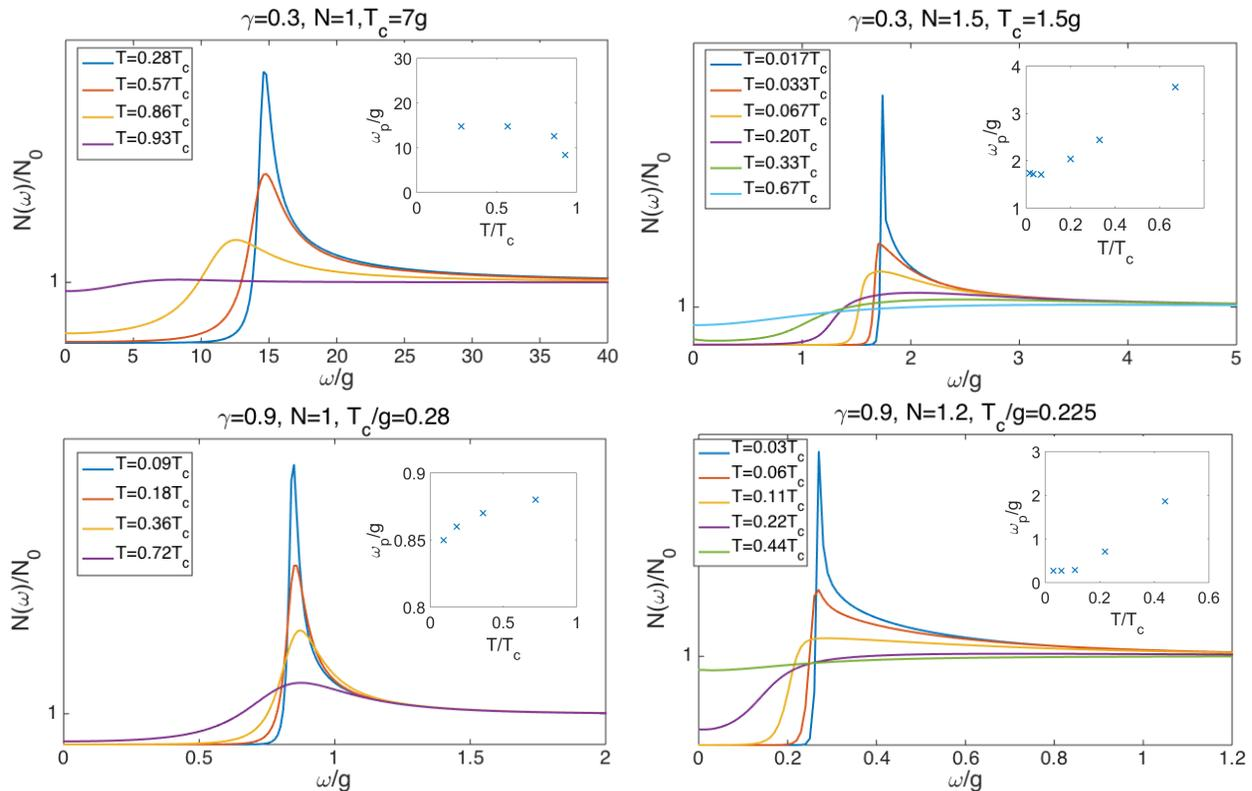


FIG. 25. DOS $N(\omega)$ as a function of frequency for $\gamma = 0.3$ and $\gamma = 0.9$ and several $N < N_{cr}(\gamma)$. At low $T < T_{cross}$, the DOS has a sharp peak at $\omega = \Delta(T)$ and nearly vanishes below the peak. At higher $T > T_{cross}$ the DOS has qualitatively the same functional form as for large N , and the peak position shifts to a higher frequency with increasing temperature. The insets: the peak position ω_p as function of T/T_c . The crossover at T_{cross} is clearly visible.

V. DISCUSSION

In this work we analyzed the interplay between the tendency towards fermionic incoherence and the tendency towards pairing near a quantum-critical point in a metal. We used the γ model of dynamical fermion-fermion interaction mediated by a critical boson with susceptibility $\chi(\Omega_m) \propto (g/|\Omega_m|)^\gamma$. We extended the model to $SU(N)$ global symmetry and used N as a parameter. At large N , the interaction in the pairing channel is smaller by $1/N$ than the one in the particle-hole channel, which gives rise to a fermionic incoherence. Earlier work by some of us and others²¹ found markedly different behavior at $T = 0$ and at a finite T . Namely, the calculations at $T = 0$ showed that superconductivity develops if

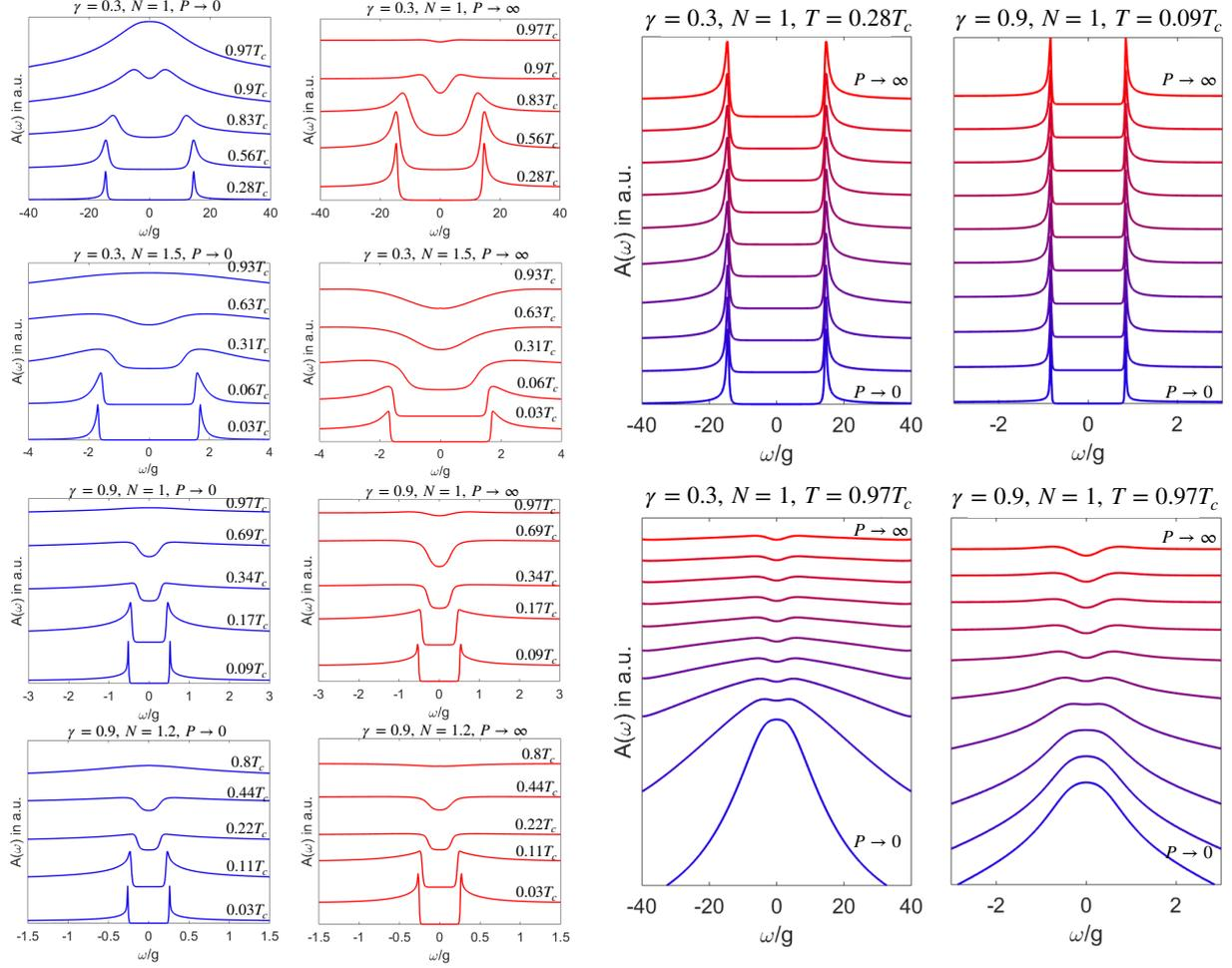


FIG. 26. The spectral function $A(\omega)$ for $\gamma = 0.3$ and $\gamma = 0.9$ and several $N < N_{cr}$. Left panels: $A(\omega)$ for a set of temperatures at either strong or weak thermal contribution (the limits $P = \infty$ and $P = 0$ in Eq. (68)). At small $T < T_{cross}$ the spectral function has sharp peaks at $\omega = \pm\Delta(T)$, like in a BCS superconductor. At $T > T_{cross}$, $A(\omega)$ shows the same behavior as the DOS in Fig. 25, when the thermal contribution is strong, and develops a single peak at $\omega = 0$ when the thermal contribution is weak. Right panels – $A(\omega)$ at a fixed T for different strengths of the thermal contribution. Upper panels – $T < T_{cross}$, lower panels – $T > T_{cross}$.

N is smaller than some γ -dependent N_{cr} , while at larger γ the system remains in a NFL normal state. On the other hand, computations of the onset temperature for the pairing $T_c(N)$ showed that $T_c(N)$ remains finite at any N and the line $T_c(N)$ by-passes N_{cr} (Fig.2). The authors of²¹ argued that this discrepancy is due to the fact that Eliashberg equations for spin-singlet pairing contain fermionic self-energy without thermal contribution (the self-

action term), and this self-energy is large (and has NFL) form for all frequencies except for $\omega_m = \pm\pi T$, at which it vanishes. The existence of a finite T_c for any N then follows from the fact that the pairing interaction between fermions with πT and $-\pi T$ is not countered by the self-energy and opens the gap Δ at these two frequencies at $T = T_c - 0$. A non-zero $\Delta(\pm\pi T)$ then induces the pairing gap for fermions with other Matsubara frequencies.

In this communication we extended the analysis of the pairing problem to $T < T_c(N)$ and solved the non-linear gap equation. We analyzed the large N limit analytically and solved the gap equation at smaller N numerically. We first obtained $\Delta(\omega_m)$ along Matsubara axis and used it to compute the Free energy and the specific heat. We found that the specific heat jumps at T_c , but at large N the relative magnitude of the jump $\Delta C(T_c - 0)/C_n(T_c)$ is smaller by a factor $1/N^2$ than in a BCS superconductor. The behavior of the specific heat below T_c is also rather unconventional, as specific heat approaches normal state form at $T \rightarrow 0$.

We then solved the gap equation along the real axis, using $\Delta(\omega_m)$ as input. We obtained $\Delta(\omega)$ and used it to compute the DOS $N(\omega)$ and the spectral function $A(\omega)$. In a conventional BCS-type superconductor $A(\omega)$ and $N(\omega)$ are peaked at the gap value $\Delta(T)$, and the peak position shifts to a smaller ω as temperature increases towards T_c (the gap “closes in”). We found that at $N > N_{cr}$, the behavior is very different – the position of the maximum in $N(\omega)$ increases linearly with T and remains finite at T_c . The DOS remains finite at all frequencies, including $\omega = 0$. At small T , $N(\omega)$ at small ω is reduced compared to $N(\omega) = N_0$ in the normal state, it displays a pseudogap behavior. As T increases towards T_c , pseudogap just “fills in”.

The form of the spectral function $A(\omega)$ depends on the strength of the thermal contribution. In our model, thermal contribution diverged at a QCP. In this limit, $A(\omega)$ has the same frequency dependence as the DOS $N(\omega)$. Away from a QCP, when the bosonic susceptibility $\chi(\Omega)$ is not singular at $\Omega = 0$, thermal contribution does not diverge. In the limit when the thermal contribution is weak, $A(\omega)$ at when $N > N_{cr}$ has a single peak at $\omega = 0$. At $N < N_{cr}$, it has two sharp peaks at $\omega \approx \pm\Delta(0)$, when $T < T_{cross}(N)$, and a single peak at $\omega = 0$ when $T > T_{cross}(N)$.

The issue we didn't discuss in this work is whether gap fluctuations (transverse and longitudinal) destroy long-range superconducting order in some T range below $T_c(N)$. Eliashberg theory, which we used, neglects gap fluctuations. It is very likely that in some range

below Eliashberg $T_c(N)$ long-range superconducting order gets destroyed, and the actual $T_{c,act} < T_c$. We note in this regard that in our theory, the transformation from “gap closing” to “gap filling” in the DOS and the spectral function at $T \sim T_{cross}(N)$ is due to the fact that at $T > T_{cross}(N)$, the feedback from the pairing on the fermionic self-energy is weak. This last result does not actually rely on the existence of long-range superconducting order. If fluctuations destroy superconducting phase coherence, the feedback will be further reduced, but we emphasize that the feedback on fermions is small above $T_{cross}(N)$ already within the Eliashberg theory. The same argument holds for the transformation from two peaks at a finite frequency in $A(\omega)$ to a single peak at $\omega = 0$.

The transformation from “gap closing” behavior at small T to “gap filling” behavior at $T \sim T_c$ has been observed in high- T_c cuprates, in the DOS⁴¹ and ARPES measurements of the spectral function in the antinodal region^{41–50}. Symmetrized data of MDC ARPES measurements along a particular direction of \mathbf{k} in the near-nodal region showed the transformation from two peaks at a finite frequency to a single peak at $\omega = 0$ (this is termed as the appearance of the Fermi arc). These results are consistent with our microscopic analysis for the DOS and also for the spectral function, if we assume that the thermal contribution is stronger in the antinodal region than in the near-nodal region. The strength of thermal contribution scales with the static bosonic susceptibility $\chi'(0)$. Static $\chi'(0)$ is larger for antinodal fermions in, e.g., spin-fluctuation models^{7,16,71}, where the interaction is peaked at momentum at or near (π, π) .

A final remark. In our analysis we didn’t include the dependence of the pairing vertex and the gap on the angle along the Fermi surface, e.g., $\cos 2\theta$ dependence for the d -wave gap in the cuprate superconductors. The d -wave form of the pairing gap does not affect our results for the DOS and $A(\omega)$ in the antinodal region, as there the gap can be approximated by the constant. We note in this regard that our results for the development of the dip with increasing T in the DOS and in the spectral function at large P , (e.g., representative results in Fig.4 and right panel in Fig.5) are quite consistent with DOS and ARPES data in the cuprates. We associate our result for smaller P (i.e., smaller thermal contribution) with the system behavior closer to the nodes. This association is valid if the pairing interaction in the cuprates is the strongest at momentum transfers connecting antinodal points and weaker at momentum transfer along the diagonals, like in spin-fluctuation scenario. Our results then show (left panel in Fig.5) that in the near-nodal regime, the two peaks, originally separated

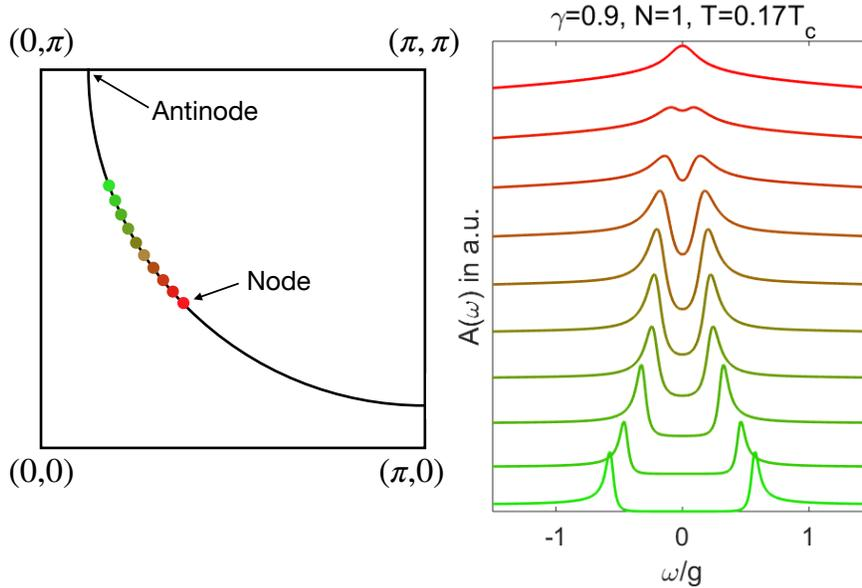


FIG. 27. The spectral function $A(\omega)$ along the Fermi surface at $T < T_{cross}$. In the nodal region (Red) $A(\omega)$ has two closely located peaks, which merge at the node. In the antinodal region (Green), the two peaks of $A(\omega)$ are well separated. We set $\gamma = 0.9, N = 1$, and $T = 0.17T_c$.

by 2Δ at a particular k -point on the Fermi surface transform into a single peak at $\omega = 0$ as T increases. This effect is well known as the development of the Fermi arc.

The modeling of the angular dependence of the gap $\Delta(\theta)$ is needed for the analysis how the spectral function evolves as a function of θ at a given T . To obtain this dependence in our data, we added $\cos 2\theta$ factor to $\Phi^*(\omega)$ and solved the Eliashberg equations at a given P, T , and γ . At high $T > T_{cross}$, the evolution is similar to the one in Fig.21. Namely, near the node $A(\omega)$ has a single maximum at $\omega = 0$, while in the antinodal region $A(\omega)$ has a dip at $\omega = 0$ and a shallow maximum, whose frequency scales with T . At $T < T_{cross}$, $A(\omega)$ has two weakly separated peaks in the nodal region and strongly separated peaks in the antinodal region (Fig.27) This behavior and the one in Fig. 26 reproduce ARPES data in Refs.^{42-44,46-50}.

ACKNOWLEDGMENTS

We thank D. Dessau, A. Millis, N. Prokofiev, S. Raghu, G. Torroba, and A. Yazdani for useful discussions. This work by Y. Wu and AVC was supported by the NSF DMR-1523036.

APPENDIX: ANALYTIC CONTINUATION FROM MATSUBARA AXIS TO REAL FREQUENCY AXIS

In this Appendix we show the derivation of Eq. (44) for the pairing vertex $\Phi^*(\omega)$ and the self-energy $\Sigma^*(\omega)$ along real frequency axis. We follow Ref.³ and use spectral decomposition approach. To avoid misunderstanding, here we explicitly keep the factors i for Matsubara frequencies, i.e. define the interaction as $\chi(i\Omega) = \frac{g^\gamma}{|\Omega|^\gamma}$. For a general complex number z the retarder $\chi(z)$ is we have

$$\chi(z) = \left(\frac{-g^2}{z^2} \right)^{\gamma/2} \quad (69)$$

Along real frequency axis ($z = \omega + i\delta$) we have

$$\begin{aligned} \text{Re } \chi(\omega) &= \frac{g^\gamma}{|\omega|^\gamma} \cos \frac{\pi\gamma}{2} \\ \text{Im } \chi(\omega) &= \frac{g^\gamma \text{sgn}(\omega)}{|\omega|^\gamma} \sin \frac{\pi\gamma}{2}. \end{aligned} \quad (70)$$

By Cauchi theorem, the susceptibility at arbitrary z can be expressed via $\text{Im } \chi(x)$ as

$$\chi(z) = (2/\pi) \int_0^\infty dx \frac{\text{Im } \chi(x)x}{(x^2 - z^2)} \quad (71)$$

Along real frequency axis this reduces to KK relation $\text{Re } \chi(\omega) = (2/\pi) \mathcal{P} \int_0^\infty dx \text{Im } \chi(x)x/(x^2 - \omega^2)$. In the calculations of $\Phi(\omega_m)$ and $\tilde{\Sigma}(\omega_m)$ we used the susceptibility $\chi(i\omega_m - i\omega_{m'})$, weighted with $\Phi(\omega_{m'})/\sqrt{\tilde{\Sigma}^2(\omega_{m'}) + \Phi^2(\omega_{m'})}$ and $\tilde{\Sigma}(\omega_m)/\sqrt{\tilde{\Sigma}^2(\omega_{m'}) + \Phi^2(\omega_{m'})}$, respectively, and summed up over $\omega_{m'}$ (Eq. 5). These expressions cannot be converted to real frequency ω by just replacing $z = i\omega_m$ by $z = \omega$ in $\chi(z - i\omega_{m'}) = (-g^2/(z - i\omega_{m'})^2)^{\gamma/2}$ because this $\chi(z)$ has branch cuts in a complex plane of z along $z = i\omega_{m'} + z_0$, where z_0 is a real variable (Ref.³). Because of this complication, we have to implement the full spectral decomposition procedure. Namely, we depart from Eliashberg equations along Matsubara axis and use spectral representation to express $G(i\omega_m, \mathbf{k})$ and $\chi(i\omega_m - i\omega_{m'})$ via $\text{Im } G(x, \mathbf{k})$ and $\text{Im } \chi(x)$

along real axis as

$$\begin{aligned} G(i\omega_m, \mathbf{k}) &= \int_{-\infty}^{\infty} \frac{dx}{\pi} \frac{\text{Im } G^R(x, \mathbf{k})}{x - i\omega_m} \\ \chi(i\omega_m - i\omega_{m'}) &= \int_{-\infty}^{\infty} \frac{dy}{\pi} \frac{\text{Im } \chi(y)}{y - i(\omega_m - \omega_{m'})} \end{aligned} \quad (72)$$

where "R" stands for "retarded". We then explicitly sum over $\omega_{m'}$ and integrate over \mathbf{k} and obtain the expressions for $\tilde{\Sigma}(i\omega_m)$ and $\Phi(i\omega_m)$, in which the dependence on ω_m is only via $1/(i\omega_m - x - y)$. This form can be straightforwardly continued analytically to real frequency by just replacing $i\omega_m$ by $\omega + i0^+$.

For compactness, we do the calculations in Nambu formalism, in which one operates with the matrix Green's function $\hat{G}(i\omega_m, \mathbf{k})$ and treats both $\Sigma(i\omega_m)$ and $\Phi(i\omega_m)$ as elements of matrix self-energy $\hat{\Sigma}(i\omega_m)$. The Eliashberg equation in Nambu formalism is

$$\hat{\Sigma}(i\omega_n) = -T \sum_m \int \frac{d^2k}{(2\pi)^2} \hat{\tau}_3 \hat{G}(i\omega_m, \mathbf{k}) \hat{\tau}_3 \chi(i\omega_n - i\omega_m), \quad (73)$$

where $\hat{\tau}_3$ is a Pauli matrix. $\hat{\Sigma} = \Sigma \hat{\tau}_0 - \Phi \hat{\tau}_1$, and the matrix $\hat{G}(i\omega_m, \mathbf{k}) = -(i\omega_m - \hat{\Sigma}(i\omega_m))^{-1}$. The diagonal and off-diagonal elements of $\hat{G}(i\omega_m, \mathbf{k})$ are conventional normal and anomalous Green's functions.

Substituting the spectral representation (72) into (73) and performing the summation over ω_m , we obtain

$$\begin{aligned} \hat{\Sigma}(i\omega_n) &= -T \sum_m \int \frac{d^2k}{(2\pi)^2} \int \frac{dx dy}{\pi^2} \hat{\tau}_3 \frac{\text{Im } \hat{G}^R(x, \mathbf{k})}{i\omega_m - x} \hat{\tau}_3 \frac{\text{Im } \chi(y)}{i\omega_n - i\omega_m - y} \\ &= - \int \frac{d^2k}{(2\pi)^2} \int \frac{dx dy}{\pi^2} \hat{\tau}_3 \text{Im } \hat{G}^R(x, \mathbf{k}) \hat{\tau}_3 \text{Im } \chi(y) \frac{1}{i\omega_n - x - y} (n_F(x) + n_B(-y)) \end{aligned} \quad (74)$$

Replacing $i\omega_n$ with $\omega + i0^+$ we obtain the self-energy at real frequencies

$$\hat{\Sigma}(\omega) = - \int \frac{d^2k}{(2\pi)^2} \int \frac{dx dy}{\pi^2} \hat{\tau}_3 \text{Im } \hat{G}^R(x, \mathbf{k}) \hat{\tau}_3 \text{Im } \chi(y) \frac{1}{\omega - x - y + i0^+} (n_F(x) + n_B(-y)) \quad (75)$$

We next express $\text{Im } \hat{G}^R(x, \mathbf{k})/(\omega - x - y + i0^+)$ via the full $\hat{G}^R(x, \mathbf{k})$ as

$$\begin{aligned} \frac{2 \text{Im } \hat{G}^R(x, \mathbf{k})}{\omega - x - y + i0^+} &= \text{Im} \left[\hat{G}^R(x, \mathbf{k}) \left(\frac{1}{\omega - x - y + i0^+} + \frac{1}{\omega - x - y - i0^+} \right) \right] \\ &\quad - i \text{Re} \left[\hat{G}^R(x, \mathbf{k}) \left(\frac{1}{\omega - x - y + i0^+} - \frac{1}{\omega - x - y - i0^+} \right) \right]. \end{aligned} \quad (76)$$

and integrate over x by closing the integration contour over the upper half-plane of complex x . Because $\hat{G}^R(x, \mathbf{k})$ is analytic in the upper half plane, the poles are at $x = \omega - y + i0^+$ and

$x = i(2n + 1)\pi T$ [these are the poles coming from $n_F(x)$]. Using the residue theorem, we find

$$\begin{aligned}
\hat{\Sigma}(\omega) &= -\frac{1}{2} \int \frac{d^2k}{(2\pi)^2} \int \frac{dy}{\pi} \text{Im} \chi(y) \\
&\times \left\{ \text{Im} \left[\int \frac{dx}{\pi} (n_F(x) + n_B(-y)) \hat{\tau}_3 \hat{G}^R(x, \mathbf{k}) \hat{\tau}_3 \left(\frac{1}{\omega - x - y + i0^+} + \frac{1}{\omega - x - y - i0^+} \right) \right] \right. \\
&\quad \left. - i \text{Re} \left[\int \frac{dx}{\pi} (n_F(x) + n_B(-y)) \hat{\tau}_3 \hat{G}^R(x, \mathbf{k}) \hat{\tau}_3 \left(\frac{1}{\omega - x - y + i0^+} - \frac{1}{\omega - x - y - i0^+} \right) \right] \right\} \\
&= \int \frac{d^2k}{(2\pi)^2} \int \frac{dy}{\pi} \text{Im} \chi(y) T \sum_{\omega_n > 0} \text{Im} \left[i \hat{\tau}_3 \hat{G}^R(i\omega_n, \mathbf{k}) \hat{\tau}_3 \left(\frac{1}{\omega - i\omega_n - y} + \frac{1}{\omega - i\omega_n - y} \right) \right] \\
&\quad + \int \frac{d^2k}{(2\pi)^2} \int \frac{dy}{\pi} \text{Im} \chi(y) (n_F(\omega - y) + n_B(-y)) \times \left[\text{Im}(i \hat{\tau}_3 G^R(\omega - y, \mathbf{k}) \hat{\tau}_3) - i \text{Re}(i \hat{\tau}_3 G^R(\omega - y, \mathbf{k}) \hat{\tau}_3) \right] \\
&= 2T \sum_{\omega_n > 0} \int \frac{d^2k}{(2\pi)^2} \int \frac{dy}{\pi} \text{Im} \chi(y) \text{Im} \frac{i \hat{\tau}_3 \hat{G}^R(i\omega_n, \mathbf{k}) \hat{\tau}_3}{\omega - i\omega_n - y} \\
&\quad + \int \frac{d^2k}{(2\pi)^2} \int \frac{dy}{\pi} \text{Im} \chi(y) \hat{\tau}_3 \hat{G}^R(\omega - y, \mathbf{k}) \hat{\tau}_3 (n_F(y - \omega) + n_B(y)), \tag{77}
\end{aligned}$$

Using now $(1/\pi) \int dy \text{Im} \chi(y)/(\omega - i\omega_m - y) = -\chi(\omega - i\omega_m)$, we finally obtain

$$\begin{aligned}
\hat{\Sigma}(\omega) &= -2T \sum_{\omega_n > 0} \int \frac{d^2k}{(2\pi)^2} \text{Im}[i \hat{\tau}_3 \hat{G}^R(i\omega_n, \mathbf{k}) \hat{\tau}_3 \chi(\omega - i\omega_n)] \\
&\quad - \int \frac{d^2k}{(2\pi)^2} \int \frac{dy}{\pi} \text{Im}[\chi(y)] \hat{\tau}_3 \hat{G}^R(\omega - y, \mathbf{k}) \hat{\tau}_3 (n_F(y - \omega) + n_B(y)). \tag{78}
\end{aligned}$$

Let's now split this matrix equation into the equations for the pairing vertex $\Phi(\omega)$ and conventional (non-anomalous) self-energy $\Sigma(\omega)$. Expressing $\hat{\Sigma}(\omega)$ as

$$\hat{\Sigma}(\omega) = \Sigma(\omega) \hat{\tau}_0 - \Phi(\omega) \hat{\tau}_1 \tag{79}$$

and substituting into the Dyson equation, we obtain

$$\hat{\tau}_3 G(\omega, \mathbf{k}) \hat{\tau}_3 = \frac{1}{\xi_{\mathbf{k}}^2 + \Phi(\omega)^2 - (\omega + \Sigma(\omega) + i0^+)^2} (-(\omega + \Sigma(\omega)) \hat{\tau}_0 - \xi_{\mathbf{k}} \hat{\tau}_3 + \Phi(\omega) \hat{\tau}_1) \tag{80}$$

where $\xi_{\mathbf{k}}$ is the fermionic dispersion. Expressing next $\int d^2k/(2\pi)^2 = N_0 \int d\xi_{\mathbf{k}}$, where N_0 is the DOS in the normal state, and integrating over $\xi_{\mathbf{k}}$, we obtain

$$\int \frac{d^2k}{(2\pi)^2} \hat{\tau}_3 G(\omega, \mathbf{k}) \hat{\tau}_3 = N_0 \int_{-\infty}^{\infty} d\xi_{\mathbf{k}} \hat{\tau}_3 G(\omega, \mathbf{k}) \hat{\tau}_3 = i\pi N_0 \frac{-\tilde{\Sigma}(\omega) \hat{\tau}_0 + \Phi(\omega) \hat{\tau}_1}{\sqrt{\tilde{\Sigma}^2(\omega) - \Phi(\omega)^2}} \tag{81}$$

where $\tilde{\Sigma}(\omega) = \omega + \Sigma(\omega)$. Absorbing the density of states N_0 into χ and splitting $\hat{\Sigma}(\omega)$ into

normal and anomalous components, we obtain

$$\begin{aligned}
\tilde{\Sigma}(\omega) &= \omega + i\pi T \sum_{\omega_m > 0} \frac{\tilde{\Sigma}(\omega_m)}{\sqrt{\Phi^2(\omega_m) + (\tilde{\Sigma}^2(\omega_m))}} (\chi(\omega_m + i\omega) - \chi(\omega_m - i\omega)) \\
&\quad + i \int dy [S_{\Sigma}(\omega - y) \text{Im } \chi(y) (n_F(y - \omega) + n_B(y))] \\
\Phi(\omega) &= \pi T \sum_{\omega_m > 0} \frac{\Phi(\omega_m)}{\sqrt{\Phi^2(\omega_m) + \tilde{\Sigma}^2(\omega_m)}} (\chi(\omega_m + i\omega) + \chi(\omega_m - i\omega)) \\
&\quad + i \int dy [S_{\Phi}(\omega - y) \text{Im } \chi(y) (n_F(y - \omega) + n_B(y))]
\end{aligned} \tag{82}$$

where

$$\begin{aligned}
S_{\Phi}(\omega) &= \frac{\Phi(\omega)}{\sqrt{\tilde{\Sigma}^2(\omega) - \Phi^2(\omega)}} = \frac{\Phi(\omega)}{\tilde{\Sigma}(\omega)} \frac{1}{\sqrt{1 - \left(\frac{\Phi(\omega)}{\tilde{\Sigma}(\omega)}\right)^2}} \\
S_{\Sigma}(\omega) &= \frac{\tilde{\Sigma}(\omega)}{\sqrt{\tilde{\Sigma}^2(\omega) - \Phi^2(\omega)}} = \frac{1}{\sqrt{1 - \left(\frac{\Phi(\omega)}{\tilde{\Sigma}(\omega)}\right)^2}}
\end{aligned} \tag{83}$$

At a finite T and small y , $n_B(y) \approx T/y$. At a QCP $\text{Im } \chi(y)n_B(y)$ then scales as $T/|y|^{1+\gamma}$, and integrals over dy in (82) diverge. The divergence, however, cancels out in the ratio $\Phi(\omega)/\tilde{\Sigma}(\omega) = \Delta(\omega)/\omega$ and can be formally eliminated by introducing new $\Phi^*(\omega)$ and $\tilde{\Sigma}^*(\omega)$ in which the divergent pieces are subtracted:

$$\begin{aligned}
\tilde{\Sigma}^*(\omega) &= \omega + i\pi T \sum_{\omega_m > 0} \frac{\tilde{\Sigma}(\omega_m)}{\sqrt{(\Phi(\omega_m))^2 + (\tilde{\Sigma}(\omega_m))^2}} (\chi(\omega_m + i\omega) - \chi(\omega_m - i\omega)) \\
&\quad + i \int dy \text{Im } \chi(y) \left[S_{\Sigma}(\omega - y) (n_F(y - \omega) + n_B(y)) - S_{\Sigma}(\omega) \frac{T}{y} \right] \\
\Phi^*(\omega) &= \pi T \sum_{\omega_m > 0} \frac{\Phi(\omega_m)}{\sqrt{(\Phi(\omega_m))^2 + (\tilde{\Sigma}(\omega_m))^2}} (\chi(\omega_m + i\omega) + \chi(\omega_m - i\omega)) \\
&\quad + i \int dy \text{Im } \chi(y) \left[S_{\Phi}(\omega - y) (n_F(y - \omega) + n_B(y)) - S_{\Phi}(\omega) \frac{T}{y} \right]
\end{aligned} \tag{84}$$

Comparing (82) and (84) we see that

$$\tilde{\Sigma}^*(\omega) = \tilde{\Sigma}(\omega)(1 - Q(\omega)), \quad \Phi^*(\omega) = \Phi(\omega)(1 - Q(\omega)), \tag{85}$$

where

$$Q(\omega) = \frac{iP}{\sqrt{\tilde{\Sigma}^2(\omega) - \Phi^2(\omega)}}, \quad P = \int_{-\infty}^{\infty} dy \text{Im } \chi(y) \frac{T}{y} = \pi T \chi(0) \tag{86}$$

The ratio $\Phi^*(\omega)/\tilde{\Sigma}^*(\omega)$ is the same as $\Phi(\omega)/\tilde{\Sigma}(\omega)$, i.e., the gap function $\Delta(\omega)$ can be equally expressed via non-singular $\Phi^*(\omega)$ and $\tilde{\Sigma}^*(\omega)$. Furthermore, a little experimentation shows

that $S_{\Phi}(\omega)$ and $S_{\Sigma}(\omega)$, given by (83), can be equally expressed via $\Phi^*(\omega)$ and $\tilde{\Sigma}^*(\omega)$, as

$$\begin{aligned} S_{\Phi}(\omega) &= \frac{\Phi^*(\omega)}{\sqrt{(\tilde{\Sigma}^*(\omega))^2 - (\Phi^*(\omega))^2}} = \frac{\Phi^*(\omega)}{\tilde{\Sigma}^*(\omega)} \frac{1}{\sqrt{1 - \left(\frac{\Phi^*(\omega)}{\tilde{\Sigma}^*(\omega)}\right)^2}} = \frac{\Delta(\omega)}{\sqrt{\omega^2 - (\Delta(\omega))^2}} \\ S_{\Sigma}(\omega) &= \frac{\tilde{\Sigma}^*(\omega)}{\sqrt{(\tilde{\Sigma}^*(\omega))^2 - (\Phi^*(\omega))^2}} = \frac{1}{\sqrt{1 - \left(\frac{\Phi^*(\omega)}{\tilde{\Sigma}^*(\omega)}\right)^2}} = \frac{\omega}{\sqrt{\omega^2 - (\Delta(\omega))^2}} \end{aligned} \quad (87)$$

By the same reason, $\Phi(\omega)$ and $\tilde{\Sigma}(\omega)$ can be expressed via $\Phi^*(\omega)$ and $\tilde{\Sigma}^*(\omega)$ in a manner similar to Eq. (85):

$$\Phi(\omega) = \Phi^*(\omega) (1 + Q^*(\omega)), \quad \tilde{\Sigma}(\omega) = \tilde{\Sigma}^*(\omega) (1 + Q^*(\omega)), \quad (88)$$

where

$$Q^*(\omega) = \frac{i\pi\chi(0)}{\sqrt{(\tilde{\Sigma}^*)^2(\omega) - (\Phi^*)^2(\omega)}} \quad (89)$$

Equations (84) are free from divergencies and can be readily extended to $N \neq 1$, as we did in the main text.

Eqs. (84) have been solved numerically by iterations. For practical purposes, we found that in some cases the convergence is faster if we do calculations in two steps: first evaluate intermediate Φ^{**} and $\tilde{\Sigma}^{**}$, related to Φ and $\tilde{\Sigma}$ as in (85), but with $P = \int_{-\delta}^{\delta} dy \operatorname{Im} \chi(y) \frac{T}{y}$, where δ is some finite number, and then compute Φ^* and Σ^* by adding the rest of the integral in P . The best convergence is achieved by adjusting the value of δ .

¹ R. Combescot, Phys. Rev. B **51**, 11625 (1995).

² Bergmann, G. and Rainer, D. Z. Physik (1973) 263: 59. P. B. Allen and D. Rainer, Nature **349**, 396 EP (1991); P. B. Allen and R. C. Dynes, Phys. Rev. B **12**, 905 (1975).

³ F. Marsiglio, M. Schossmann, and J. P. Carbotte, Phys. Rev. B **37**, 4965 (1988); F. Marsiglio and J. P. Carbotte, Phys. Rev. B **43**, 5355 (1991), for more recent results see F. Marsiglio and J.P. Carbotte, “Electron-Phonon Superconductivity”, in “The Physics of Conventional and Unconventional Superconductors”, Bennemann and Ketterson eds., Springer-Verlag, (2006) and references therein.

⁴ A. Karakozov, E. Maksimov, and A. Mikhailovsky, Solid State Communications **79**, 329 (1991).

⁵ N. E. Bonesteel, I. A. McDonald, and C. Nayak, Phys. Rev. Lett. **77**, 3009 (1996).

- ⁶ A. Abanov, A. V. Chubukov, and A. M. Finkel'stein, EPL (Europhysics Letters) **54**, 488 (2001).
- ⁷ A. Abanov, A. V. Chubukov, and J. Schmalian, Advances in Physics **52**, 119 (2003); A. Abanov and A. V. Chubukov, Phys. Rev. Lett. **83**, 1652 (1999).
- ⁸ A. Abanov, A. V. Chubukov, and S. J., Journal of Electron spectroscopy and related phenomena **117**, 129 (2001).
- ⁹ D. T. Son, Phys. Rev. D **59**, 094019 (1999); A. V. Chubukov and J. Schmalian, Phys. Rev. B **72**, 174520 (2005).
- ¹⁰ S.-S. Lee, Phys. Rev. B **80**, 165102 (2009); D. Dalidovich and S.-S. Lee, Phys. Rev. B **88**, 245106 (2013).
- ¹¹ S. Sachdev, M. A. Metlitski, Y. Qi, and C. Xu, Phys. Rev. B **80**, 155129 (2009); E. G. Moon and S. Sachdev, Phys. Rev. B **80**, 035117 (2009).
- ¹² E.-G. Moon and A. Chubukov, Journal of Low Temperature Physics **161**, 263 (2010).
- ¹³ M. A. Metlitski and S. Sachdev, Phys. Rev. B **82**, 075127 (2010); Phys. Rev. B **82**, 075128 (2010).
- ¹⁴ D. F. Mross, J. McGreevy, H. Liu, and T. Senthil, Phys. Rev. B **82**, 045121 (2010).
- ¹⁵ R. Mahajan, D. M. Ramirez, S. Kachru, and S. Raghu, Phys. Rev. B **88**, 115116 (2013); A. L. Fitzpatrick, S. Kachru, J. Kaplan, and S. Raghu, Phys. Rev. B **88**, 125116 (2013); Phys. Rev. B **89**, 165114 (2014); G. Torroba and H. Wang, Phys. Rev. B **90**, 165144 (2014); A. L. Fitzpatrick, G. Torroba, and H. Wang, Phys. Rev. B **91**, 195135 (2015), and references therein.
- ¹⁶ P. Monthoux, D. Pines, and G. G. Lonzarich, Nature **450**, 1177 (2007); D. J. Scalapino, Rev. Mod. Phys. **84**, 1383 (2012).
- ¹⁷ M.R. Norman in "Novel Superconductors", Bennemann and Ketterson eds., Oxford University Press (2014), and references therein. S. Maiti and A. V. Chubukov in "Novel Superconductors", Bennemann and Ketterson eds., Oxford University Press (2014), and references therein. L. Fratino, P. SÅlmon, G. Sordi, and A.-M. S. Tremblay, Scientific Reports **6**, 22715 (2016).
- ¹⁸ M. A. Metlitski, D. F. Mross, S. Sachdev, and T. Senthil, Phys. Rev. B **91**, 115111 (2015); K. B. Efetov, H. Meier, and C. Pepin, Nature Physics **9**, 442 (2013).
- ¹⁹ Y. Wang and A. V. Chubukov, Phys. Rev. Lett. **110**, 127001 (2013); A. V. Chubukov and P. Wölfle, Phys. Rev. B **89**, 045108 (2014).
- ²⁰ S. Raghu, G. Torroba, and H. Wang, Phys. Rev. B **92**, 205104 (2015).
- ²¹ Y. Wang, A. Abanov, B. L. Altshuler, E. A. Yuzbashyan, and A. V. Chubukov, Phys. Rev.

- Lett. **117**, 157001 (2016).
- ²² S. Lederer, Y. Schattner, E. Berg, and S. A. Kivelson, Phys. Rev. Lett. **114**, 097001 (2015).
- ²³ A. M. Tsvelik, Phys. Rev. B **95**, 201112 (2017).
- ²⁴ M. Vojta and S. Sachdev, Phys. Rev. Lett. **83**, 3916 (1999).
- ²⁵ E. Fradkin, S. A. Kivelson, M. J. Lawler, J. P. Eisenstein, and A. P. Mackenzie, Annual Review of Condensed Matter Physics **1**, 153 (2010).
- ²⁶ J. M. Bok, J. J. Bae, H.-Y. Choi, C. M. Varma, W. Zhang, J. He, Y. Zhang, L. Yu, and X. J. Zhou, Science Advances **2** (2016), 10.1126/sciadv.1501329.
- ²⁷ T. Shibauchi, A. Carrington, and Y. Matsuda, Annual Review of Condensed Matter Physics **5**, 113 (2014).
- ²⁸ D. Vilaridi, C. Taranto, and W. Metzner, arXiv:1810.02290 and references therein (2018).
- ²⁹ M. H. Gerlach, Y. Schattner, E. Berg, and S. Trebst, Phys. Rev. B **95**, 035124 (2017); Y. Schattner, S. Lederer, S. A. Kivelson, and E. Berg, Phys. Rev. X **6**, 031028 (2016); X. Wang, Y. Schattner, E. Berg, and R. M. Fernandes, Phys. Rev. B **95**, 174520 (2017).
- ³⁰ K. Haule and G. Kotliar, Phys. Rev. B **76**, 104509 (2007); W. Xu, G. Kotliar, and A. M. Tsvelik, Phys. Rev. B **95**, 121113 (2017); G. Sordi, P. Simon, K. Haule, and A.-M. S. Tremblay, Phys. Rev. Lett. **108**, 216401 (2012).
- ³¹ A. Georges, L. d. Medici, and J. Mravlje, Annu. Rev. Condens. Matter Phys. **4**, 137 (2013); W. Wu, M. Ferrero, A. Georges, and E. Kozik, Phys. Rev. B **96**, 041105 (2017).
- ³² D. V. Khveshchenko and W. F. Shively, Phys. Rev. B **73**, 115104 (2006).
- ³³ T.-H. Lee, A. Chubukov, H. Miao, and G. Kotliar, arXiv **1805**, 10280 (2018); Y.-M. Wu, Ar. Abanov, and A. V. Chubukov, arXiv:1811.02087.
- ³⁴ J. Rech, C. Pépin, and A. V. Chubukov, Phys. Rev. B **74**, 195126 (2006).
- ³⁵ There is a large body of literature on QCP with $q = 0$. For recent works, see; S. Sur and S.-S. Lee, Phys. Rev. B **91**, 125136 (2015); M. Punk, Phys. Rev. B **91**, 115131 (2015), and references therein.
- ³⁶ A. Abanov, A. V. Chubukov, and M. R. Norman, Phys. Rev. B **78**, 220507 (2008).
- ³⁷ B. L. Altshuler, L. B. Ioffe, and A. J. Millis, Phys. Rev. B **52**, 5563 (1995); D. Bergeron, D. Chowdhury, M. Punk, S. Sachdev, and A.-M. S. Tremblay, Phys. Rev. B **86**, 155123 (2012); Y. Wang and A. Chubukov, Phys. Rev. B **88**, 024516 (2013).
- ³⁸ D. J. Scalapino, Rev. Mod. Phys. **84**, 1383 (2012); S. Lederer, Y. Schattner, E. Berg, and S. A.

- Kivelson, Proceedings of the National Academy of Sciences **114**, 4905 (2017).
- ³⁹ P. Anderson, Journal of Physics and Chemistry of Solids **11**, 26 (1959).
- ⁴⁰ A. A. Abrikosov and L. P. Gor'kov, JETP **9**, 220 (1959).
- ⁴¹ O. Fischer, M. Kugler, I. Maggio-Aprile, C. Berthod, and C. Renner, Rev. Mod. Phys. **79**, 353 (2007).
- ⁴² T. J. Reber, N. C. Plumb, Z. Sun, Y. Cao, Q. Wang, K. McElroy, H. Iwasawa, M. Arita, J. S. Wen, Z. J. Xu, G. Gu, Y. Yoshida, H. Eisaki, Y. Aiura, and D. S. Dessau, Nature Physics **8**, 606 EP (2012).
- ⁴³ T. Kondo, A. D. Palczewski, Y. Hamaya, T. Takeuchi, J. S. Wen, Z. J. Xu, G. Gu, and A. Kaminski, Phys. Rev. Lett. **111**, 157003 (2013); T. Kondo, A. F. Santander-Syro, O. Copie, C. Liu, M. E. Tillman, E. D. Mun, J. Schmalian, S. L. Bud'ko, M. A. Tanatar, P. C. Canfield, and A. Kaminski, Phys. Rev. Lett. **101**, 147003 (2008).
- ⁴⁴ A. Kanigel, M. R. Norman, M. Randeria, U. Chatterjee, S. Souma, A. Kaminski, H. M. Fretwell, S. Rosenkranz, M. Shi, T. Sato, T. Takahashi, Z. Z. Li, H. Raffy, K. Kadowaki, D. Hinks, L. Ozyuzer, and J. C. Campuzano, Nature Physics **2**, 447 EP (2006); A. Kanigel, U. Chatterjee, M. Randeria, M. R. Norman, S. Souma, M. Shi, Z. Z. Li, H. Raffy, and J. C. Campuzano, Phys. Rev. Lett. **99**, 157001 (2007); H. Ding, J. C. Campuzano, A. F. Bellman, T. Yokoya, M. R. Norman, M. Randeria, T. Takahashi, H. Katayama-Yoshida, T. Mochiku, K. Kadowaki, and G. Jennings, Phys. Rev. Lett. **74**, 2784 (1995).
- ⁴⁵ J.C. Campuzano, M.R. Norman, and M. Randeria "Photoemission in the high- T_c superconductors", in "Novel Superconductors", v.2, K.H. Bennemann and J.B. Ketterson eds, Springer 2008.
- ⁴⁶ A. Damascelli, Z. Hussain, and Z.-X. Shen, Rev. Mod. Phys. **75**, 473 (2003); M. Hashimoto, I. M. Vishik, R.-H. He, T. P. Devereaux, and Z.-X. Shen, Nature Physics **10**, 483 EP (2014), review Article.
- ⁴⁷ P. D. Johnson, T. Valla, A. V. Fedorov, Z. Yusof, B. O. Wells, Q. Li, A. R. Moodenbaugh, G. D. Gu, N. Koshizuka, C. Kendziora, S. Jian, and D. G. Hinks, Phys. Rev. Lett. **87**, 177007 (2001).
- ⁴⁸ A. A. Kordyuk and S. V. Borisenko, Low Temperature Physics **32**, 298 (2006); A. A. Kordyuk, Low Temperature Physics **41**, 319 (2015).
- ⁴⁹ Y. He, Y. Yin, M. Zech, A. Soumyanarayanan, M. M. Yee, T. Williams, M. C. Boyer, K. Chat-

- terjee, W. D. Wise, I. Zeljkovic, T. Kondo, T. Takeuchi, H. Ikuta, P. Mistark, R. S. Markiewicz, A. Bansil, S. Sachdev, E. W. Hudson, and J. E. Hoffman, *Science* **344**, 608 (2014).
- ⁵⁰ Y. Peng, J. Meng, D. Mou, J. He, L. Zhao, Y. Wu, G. Liu, X. Dong, S. He, J. Zhang, X. Wang, Q. Peng, Z. Wang, S. Zhang, F. Yang, C. Chen, Z. Xu, T. K. Lee, and X. J. Zhou, *Nature Communications* **4**, 2459 EP (2013), article.
- ⁵¹ A. V. Balatsky, I. Vekhter, and J.-X. Zhu, *Rev. Mod. Phys.* **78**, 373 (2006); M. L. Kulić and O. V. Dolgov, *Phys. Rev. B* **60**, 13062 (1999); A. F. Kemper, D. G. S. P. Doluweera, T. A. Maier, M. Jarrell, P. J. Hirschfeld, and H.-P. Cheng, *Phys. Rev. B* **79**, 104502 (2009).
- ⁵² M. R. Norman, H. Ding, M. Randeria, J. C. Campuzano, T. Yokoya, T. Takeuchi, T. Takahashi, T. Mochiku, K. Kadowaki, P. Guptasarma, and D. G. Hinks, *Nature* **392**, 157 EP (1998); M. R. Norman, M. Randeria, H. Ding, and J. C. Campuzano, *Phys. Rev. B* **57**, R11093 (1998); M. Franz and A. J. Millis, *Phys. Rev. B* **58**, 14572 (1998); A. Paramekanti and E. Zhao, *Phys. Rev. B* **75**, 140507 (2007); E. Berg and E. Altman, *Phys. Rev. Lett.* **99**, 247001 (2007), and references therein.
- ⁵³ A. V. Chubukov, M. R. Norman, A. J. Millis, and E. Abrahams, *Phys. Rev. B* **76**, 180501 (2007).
- ⁵⁴ A. A. Abrikosov and L. P. Gor'kov, *JETP* **12**, 227 (1961).
- ⁵⁵ K. Maki, *Physics Physique Fizika* **1**, 21 (1964); P. Fulde and K. Maki, *Phys. Rev. Lett.* **15**, 675 (1965); Y. WADA, *Rev. Mod. Phys.* **36**, 253 (1964); D. J. Scalapino, Y. Wada, and J. C. Swihart, *Phys. Rev. Lett.* **14**, 102 (1965).
- ⁵⁶ J. Fink, A. Koitzsch, J. Geck, V. Zabolotnyy, M. Knupfer, B. Büchner, A. Chubukov, and H. Berger, *Phys. Rev. B* **74**, 165102 (2006).
- ⁵⁷ A. Abanov and A. V. Chubukov, *Phys. Rev. Lett.* **83**, 1652 (1999).
- ⁵⁸ M. Eschrig, *Advances in Physics* **55**, 47 (2006).
- ⁵⁹ J. M. Luttinger and J. C. Ward, *Phys. Rev.* **118**, 1417 (1960).
- ⁶⁰ R. Haslinger and A. V. Chubukov, *Phys. Rev. B* **68**, 214508 (2003).
- ⁶¹ A. J. Millis, S. Sachdev, and C. M. Varma, *Phys. Rev. B* **37**, 4975 (1988).
- ⁶² A. A. Abrikosov, L. P. Gorkov, and I. E. Dzyaloshinski, *Methods of Quantum Field Theory in Statistical Physics*, 2nd edition, (Pergamon Oxford, 1965).
- ⁶³ Z. Wang, W. Mao, and K. Bedell, *Phys. Rev. Lett.* **87**, 257001 (2001); R. Roussev and A. J. Millis, *Phys. Rev. B* **63**, 140504 (2001); A. V. Chubukov, A. M. Finkel'stein, R. Haslinger, and

- D. K. Morr, Phys. Rev. Lett. **90**, 077002 (2003).
- ⁶⁴ A. J. Millis, Phys. Rev. B **45**, 13047 (1992).
- ⁶⁵ C. Castellani, C. Di Castro, and M. Grilli, Phys. Rev. Lett. **75**, 4650 (1995); A. Perali, C. Castellani, C. Di Castro, and M. Grilli, Phys. Rev. B **54**, 16216 (1996); S. Andergassen, S. Caprara, C. Di Castro, and M. Grilli, Phys. Rev. Lett. **87**, 056401 (2001).
- ⁶⁶ D. Chowdhury and S. Sachdev, Phys. Rev. B **90**, 134516 (2014); Phys. Rev. B **90**, 245136 (2014); Y. Wang and A. V. Chubukov, Phys. Rev. B **92**, 125108 (2015).
- ⁶⁷ J. Bardeen and M. Stephen, Phys. Rev. **136**, A1485 (1964).
- ⁶⁸ G. M. Eliashberg, JETP **11**, 696 (1960).
- ⁶⁹ Note that $\Delta^R(\omega) \propto i\omega$ should not be confused with odd-frequency pairing. When expressed in time-ordered operators at real frequencies, $\Delta(\omega) \propto i|\omega|$ which is even in frequency.
- ⁷⁰ A. V. Chubukov, I. Eremin, and D. V. Efremov, Phys. Rev. B **93**, 174516 (2016).
- ⁷¹ D.J. Scalapino in Ref.38.